

UNIVERSITY OF CINCINNATI

Date: _____

I, _____,
hereby submit this work as part of the requirements for the degree of:

in:

It is entitled:

This work and its defense approved by:

Chair: _____

FEASIBILITY STUDY OF THERMAL-ELASTOGRAPHIC DETECTION OF NON-VOIDED HARD-ALPHA INCLUSIONS IN TITANIUM ALLOYS

A thesis submitted to the

Division of Research and Advanced Studies
of the University of Cincinnati

in partial fulfillment of the
requirements for the degree of

MASTER OF SCIENCE

in the Department of Aerospace Engineering
and Engineering Mechanics
of the College of Engineering

2004

by

Kevin Kramer

B.S. Engineering Mechanics, University of Cincinnati, 2003

Committee Chair: Dr. Peter B. Nagy

ABSTRACT

Hard-alpha inclusions are low-density, hard, brittle regions of spuriously high nitrogen and oxygen content that occur in titanium alloys. Usually, these inclusions are cracked or include voids, so they are easy to detect by ultrasonic means. The difficulty for ultrasonic NDT is detecting the uncracked hard-alpha inclusions. This problem is very critical to research since titanium alloys are used in aircraft engines and the material is made more brittle and subject to failure with the added nitrogen and oxygen content. The purpose of this research is to study the feasibility of novel ultrasonic methods to identify nitrogen-enriched regions in titanium alloy components.

The three methods studied in this project include thermal expansion, acousto-elastic, and acousto-thermal tests. Our nondestructive measurements provide information on the relevant physical properties of specimens without excess nitrogen content and ones with nitrogen levels ranging from 2.5% - 5.9%. Based on our measurements, the direct thermal expansion effect and the thermally induced acousto-elastic effect are all but negligible relative to the acousto-thermal velocity change. The longitudinal and shear acousto-thermal coefficients were found to be rather sensitive to changes in nitrogen content. Both the longitudinal and shear acousto-thermal coefficients are negative, i.e., the velocities decrease at increasing temperatures. According to our results, the longitudinal coefficient decreases while the shear coefficient increases with increasing nitrogen content. Hopefully, these results can help identify an ultrasonic test method that can detect material inclusions with a level of nitrogen that could be detrimental to an aircraft engine.

ACKNOWLEDGEMENTS

This work was supported by the U.S. Department of Transportation, Federal Aviation Administration (DOT/FAA/AR-480) through a subcontract from Honeywell Engines, Systems, and Services of Phoenix, AZ. The author would like to express his appreciation to Dr. Waled Hassan of Honeywell Engines, Systems, and Services for his valuable technical contributions to this project. Also, special thanks go to Dr. Peter B. Nagy for his guidance and technical advice throughout the entirety of this work, as well as the other members of the thesis committee, Dr. James Wade and Dr. Jandro Abot. The Ti-N specimens used in this study were originally manufactured at the Global Research Center of General Electric, Schenectady, NY, and were provided for this effort by the Metals, Ceramics, and NDE Branch of the Air Force Research Laboratory (MLLP AFRL) of Dayton, OH.

LIST OF FIGURES

Figure 1.	Principal directions of the acousto-elastic effect in isotropic materials.	23
Figure 2.	Reading from TIC versus time, showing drift of signal due to temperature fluctuations.	24
Figure 3.	Relative velocity change versus stress in Al-1100-H14 using a longitudinal transducer.	27
Figure 4.	Relative velocity change versus stress in Al-1100-H14 using a shear transducer.	27
Figure 5.	Relative velocity change versus stress in Al-4032-T6 using a longitudinal transducer.	28
Figure 6.	Relative velocity change versus stress in Al-4032-T6 using a shear transducer.	28
Figure 7.	Apparent velocity change versus temperature in Al-1100-H14 using a longitudinal transducer.	31
Figure 8.	Apparent velocity change versus temperature in Al-4032-T6 using a longitudinal transducer.	31
Figure 9.	A schematic diagram of the thermal expansion measurements.	33
Figure 10.	Experimental setup for thermal expansion measurements.	33
Figure 11.	Explanation of positive and negative zero crossings to use for time measurements.	35
Figure 12.	A schematic diagram of the acousto-elastic measurements.	37
Figure 13.	Experimental setup for acousto-elastic measurements.	37

Figure 14.	A schematic diagram of the acousto-thermal measurements.	40
Figure 15.	Experimental setup for acousto-thermal measurements.	40
Figure 16.	PLC versus temperature for titanium with varying levels of nitrogen content.	44
Figure 17.	ACE versus temperature for titanium with varying levels of nitrogen content.	44
Figure 18.	Relative velocity change versus stress in Al-2024 using a longitudinal transducer.	49
Figure 19	Relative velocity change versus stress in Al-2024 using a shear transducer.	49
Figure 20.	Relative velocity change versus stress in Ti-6Al-4V using a longitudinal transducer.	50
Figure 21.	Relative velocity change versus stress in Ti-6Al-4V using a shear transducer.	50
Figure 22.	Apparent velocity change versus temperature in titanium with 3.1% N using a longitudinal transducer (acceptable data).	53
Figure 23.	Apparent velocity change versus temperature in titanium with 3.1% N using a longitudinal transducer (unacceptable data).	53
Figure 24.	Distribution of the coefficient of determination (R^2) versus the longitudinal acousto-thermal coefficient (β) after eliminating the few obvious artifacts of $R^2 < 0.95$.	54
Figure 25.	A graphical representation of the longitudinal acousto-thermal coefficient data listed in Table 5 (the error bars indicate the	

	full range of the measured values).	55
Figure 26.	Longitudinal velocity in titanium with varying levels of nitrogen content.	58
Figure 27.	Shear velocity in titanium with varying levels of nitrogen content.	58
Figure 28.	Longitudinal velocity versus increasing nitrogen content.	59
Figure 29.	Peak-to-peak amplitude of the 1” titanium specimens.	59
Figure A2.1.	Peak-to-peak amplitude versus time of a specimen placed in a room-temperature water bath using honey as the shear wave couplant.	70

TABLE OF CONTENTS

ABSTRACT	2
ACKNOWLEDGEMENTS	3
LIST OF FIGURES	4
TABLE OF CONTENTS	7
1. Introduction	9
1.1 Hard-Alpha Inclusions	9
1.2 Elastography	13
1.3 Thermal-Elastography	14
1.3.1 Thermal Expansion	15
1.3.1.1 Nature of Thermal Expansion	15
1.3.1.2 Early History	15
1.3.1.3 Modern Thermal Expansion Measurements	17
1.3.1.4 Pushrod Dilatometers	18
1.3.1.5 Reference Materials and Sample Sizes	19
1.3.2 An Illustration: Al-1100-H14 versus Al-4032-T6	21
1.3.2.1 Acousto-Elastic Effect	22
1.3.2.2 Acousto-Thermal Effect	29
2. Experimental Setup	32
2.1 Thermal Expansion Measurements	32
2.2 Acousto-Elastic Measurements	34
2.3 Acousto-Thermal Measurements	38
3. Results	41

3.1	Thermal Expansion Coefficient	41
3.2	Acousto-Elastic Coefficient	45
3.3	Acousto-Thermal Coefficient	51
3.4	Velocity Measurements	56
4.	Relative Contributions to the Overall Thermal Effect	60
5.	Conclusions	63
6.	Future Work	64
7.	Bibliography	66
8.	Appendix	68
8.1	Appendix 1: Detailed Setup for Time Delay Measurements	68
8.2	Appendix 2: Acousto-Thermal Shear Wave Couplant Study	69

1. Introduction

1.1 Hard-alpha Inclusions

Hard-alpha inclusions are also known as high interstitial defects and are regions of much higher hardness than the surrounding material. The increased brittleness of alpha inclusions is the result of excess nitrogen and oxygen that increase the beta transus of the material. These inclusions may appear during the manufacturing process if the starting material is already contaminated, if the proper temperature is not maintained to break up the alpha regions, or the material becomes contaminated during the melt process [1].

The hard-alpha titanium with the added nitrogen is much more brittle than the base metal, and a study was done to experimentally show the transition from plastic deformation to brittle fracture. It was concluded that titanium with nitrogen content less than 4 weight percentage is ductile and exhibits plastic deformation while titanium with nitrogen content at 5.5 weight percentage or greater is brittle and exhibits brittle fracture [2]. This creates much concern since brittle fracture of a turbine blade is detrimental to an aircraft engine.

However, these hard-alpha cases are extremely rare. These defects can be characterized as low frequency, high impact occurrences because they can reduce minimum fatigue life by an order of magnitude, but are only seen once in every two to three million pounds of premium quality billet [3]. Nonetheless, engines have failed because of hard-alpha inclusions, like the Sioux City crash in 1989.

United Airlines Flight 232 crashed on July 19, 1989, and killed 112 people while injuring 171. The flight originated from Denver, Colorado, and crashed while attempting to land at Sioux City Gateway Airport. One of the three GEAE CF6-6 engines failed while cruising at 37,000 feet and in turn, caused the three redundant hydraulic flight control systems to fail. The crew

was able to control the plane partially with the other engines, but eventually crashed in Sioux City [4]. In October of 1989, pieces of the engine were found 70 miles east of Sioux City, namely the fan disk with blades attached. The separation of this fan rotor disk was determined to be the cause of the engine failure [5].

The titanium alloy ingot used for the fan rotor disk was some of the last material to go through double-vacuum melting. Shortly after, General Electric changed specifications to triple-vacuum melting. The disk went through all of the normal inspections and was acceptable. The official cause of the separation of the rotor disk was the result of a fatigue crack that started from a hard-alpha defect on the surface [5]. Numerous questions arose then as to when the defect initially occurred and why it was not detected at manufacture or any of the previous inspections. The final consensus was that not enough consideration was given to human factors limitations in the inspection procedures of United Airlines overhaul facility which resulted in a failure to detect an inclusion in a crucial aspect of a rotating part [6].

Soon after, the National Transportation Safety Board (NTSB) suggested numerous improvements to the Federal Aviation Administration (FAA). Among these were to intensify nondestructive inspection research, mandate service life limits of parts, develop an alternate method of inspecting the fan rotor disks for the presence of surface cracks, and to require the manufacturers to perform a surface inspection of critical rotating components during the manufacturing process [5]. As a response to the NTSB, the FAA created the Titanium Consortium in 1993 to provide the FAA and engine manufacturers reliable and cost-effective methods of detecting cracks and inclusions in titanium components. The Consortium was composed of a team of researchers from Iowa State University, Allied Signal Propulsion Engines-Garrett, General Electric Aircraft Engines, and Pratt and Whitney [7].

Currently, hard-alpha inclusions can be detected only if they contain cracks or voids. This means that uncracked and non-voided hard-alpha inclusions go undetected and represent a major hidden problem. Present technology for ultrasonic detection of defects includes a multi-zone system that uses multiple channels employing focused transducers and analog electronics. It uses four to eight transducers of 5 MHz each focused at a different depth in the material, thus inspecting the material uniformly [8]. Another current method for detection is Photon Induced Positron Annihilation (PIPA) developed by Positron Systems. This method promises to detect smaller, buried inclusions that other nondestructive methods cannot detect. The principle of PIPA involves penetrating the material with a photon beam to create positrons. The positrons are attracted to the defects and when they eventually collide with electrons in the material and are destroyed, gamma ray energy is released. This energy is distinct and readable and allows for characterization of the defect. With this method, defects can be detected in their earliest stage before any failure can occur [9].

The purpose of this investigation was to suggest nondestructive methods of characterizing nitrogen-enriched specimens that are free from cracks and voids. Although every weight percent of nitrogen was found to increase the sound velocity by roughly 3%, therefore the absolute acoustic impedance contrast is expected to be substantial (10-15%), the actual signal-to-noise ratio is badly limited by three adverse effects. First, the nitrogen content varies gradually towards the center of the inclusion therefore the reflected signal remains rather weak. Second, the shape of the inclusion is typically very irregular; therefore the flaw signal is further reduced by random geometrical scattering effects. Third, the competing grain noise is frequently very high because of the often-coarse microstructure of the surrounding material. As a result, the backscattered ultrasonic signal from the hard-alpha inclusion is usually indistinguishable from

the incoherent material noise based on its strength alone and the probability of its detection remains inherently low [10].

Supplied by MLLP of AFRL were five titanium specimens of different nitrogen content, namely 2.5%, 3.1%, 3.8%, 4.8%, and 5.9%. Also, for comparison, titanium billet and Ti-6Al-4V forged and canted specimens were provided by Honeywell Engines. Our tests performed on these specimens are described in detail later in this paper. The Ti-N samples are representative of Ti-6Al-4V engine material since when nitrogen enters Ti-6Al-4V, the aluminum and vanadium is mostly replaced with nitrogen, thus leaving a mostly Ti-N inclusion like the specimens used in this investigation. In a study of hard-alpha defects in Ti-6Al-4V, the modified alpha phase composition at the defect center was measured to be 0.4 to 5.0 weight percentage aluminum and 0.5 to 3.1 weight percentage vanadium, compared to 5.5 to 7.2 weight percentage aluminum and 1.4 to 2.8 weight percentage vanadium in the alpha phase of the base alloy [11].

1.2 Elastography

Many cancers are identified by changes in tissue elasticity. Cancer of the breast appears as hard nodules, resulting from increased stromal density. Detection of these areas is limited by ultrasound because they are either very small or located deep within the tissue [12].

The objective of this thesis is to investigate the feasibility of a new ultrasonic NDT method aimed at detecting hard-alpha inclusions in titanium billets. Our method is based on the basic principle of elastography, a relatively new ultrasonic imaging technique, which produces images of the internal strains produced in a soft-tissue target resulting from a small external displacement of the tissue [13]. The technique can detect both soft and hard inclusions in a highly heterogeneous medium that are highly inhomogeneous themselves. Under these conditions, conventional sonography, based on the strength of ultrasonic backscattering alone, cannot be used to detect the inclusion with the required high level of confidence, a situation that is very similar to the one faced during the detection of hard-alpha inclusions in highly inhomogeneous titanium alloys. In relatively compliant soft tissue, sufficient local displacements can be produced by a quasi-static external stress field so that local strains, and thereby the local elastic stiffness, can be estimated from differential ultrasonic speckle displacements. The processed strain image is called an elastogram that has been shown to offer dramatically better detectability of scattering inclusions than the conventional sonogram itself. This technique has been primarily aimed at biomedical diagnostic applications where the elastic deformation is both substantial and easy to produce [10].

1.3 Thermal-Elastography

A similar elastographic approach based on external deformation of large pieces of structural metals like a Ti-6Al-4V billet would require tremendous external forces and would still result in minuscule contrast because, as indicated by the mere 10-15% variation in sound velocity, the elastic stiffness of the brittle inclusion is only about 20-30% higher than that of the surrounding intact material. According to the modified elastographic approach, the local strain is produced by heating the specimen. The observed shift in the grain speckle is then a combination of the increasing propagation distance caused by thermal expansion and the decreasing sound velocity caused by the temperature-dependence of the sound velocity (these two effects are actually related through the elastic nonlinearity of the material). In Ti-6Al-4V, a modest 100°C increase in temperature produces approximately 0.1% thermal expansion and almost as much as 1% drop in sound velocity. Although the absolute change in propagation time due to the thermal strain and the temperature-dependence of the sound velocity is probably comparable to what one could achieve by external mechanical loading as a result of the corresponding elastic strain and the stress-dependence of the sound velocity, the thermal loading method is inherently simpler. More importantly, the relevant physical contrast mechanism is thermal rather than elastic. To the best of our knowledge, this contrast mechanism has never been investigated before in the scientific literature. However, indirect evidence available in the published literature as well as our own preliminary measurements suggest that the variation in thermal expansion and velocity coefficients are substantially, probably as much as one order of magnitude, stronger than in the corresponding elastic coefficients. This is not surprising based on the fact that the nitrogen and oxygen contamination induced hardening and embrittlement is a nonlinear rather than linear effect on the mechanical properties of the material [10].

1.3.1 Thermal Expansion

1.3.1.1 Nature of Thermal Expansion

Thermal expansion is defined as the increase in dimensions of most substances on heating at constant pressure. However, some substances, such as tetrahedrally bonded crystals, can contract upon heating, and moreover, some solids can expand in some directions and contract in others. The general, crude explanation for thermal expansion is that central forces exist between atoms, and the mean distance between these atoms increases when they vibrate along the potential energy well line. This theory does not explain why some substances contract on heating and takes into account only the longitudinal component of motion, but it does give the most important cause of thermal expansion [14].

1.3.1.2 Early History

Long ago it was recognized that fire had an effect on the other basic elements, air, water, and earth. Countless devices were conceived from the ideas that air and water expanded and contracted upon heating and cooling. One apparatus invented by Heron of Alexandria was a mechanism based on the expansion of air that automatically opened a set of doors when a fire was lit on an altar in a temple. Similar inventions proceeded in the centuries later and eventually, the thought of relating temperature to air expansion was developed with the invention of the gas thermometer by Galileo Galilei in the seventeenth century. Major developments followed with liquid-in-glass thermometers that used water and later, alcohol, for temperature measurement. Finally, mercury was substituted for alcohol and in 1714, German physicist G.B. Fahrenheit developed a precision liquid-in-glass thermometer using mercury. These are some of the early developments in thermal science and are essentially the beginnings that led to

developments in measuring very small displacements in solids. Temperature was important to scientists because it was recognized as a characteristic of the human body and temperature measurement became essential because of the influences of temperature on substances, namely thermal expansion [15].

The first demonstration of the thermal expansion of solids was by W.J. Gravesande, who passed a brass sphere through a brass ring at room temperature, but then showed the ring to prevent passage after the sphere was heated. Thermal expansion also emerged in time precision measurements. It was found that in pendulum clocks, the period of the pendulum critically depended on its length. If the temperature drifted, the length of the pendulum would change and ultimately effect the period of the clock. Corrections had to be made for the thermal expansion of the pendulum material [15].

Petrus van Musschenbrok invented a dilatometer that measured the expansion of horizontally mounted specimens by a simple gear train in the 1730s. He reported thermal expansion data on iron, steel, copper, brass, tin, and lead. With the inventions of the lever, the rack and pinion, and the micrometer screw, the progress of thermal expansion furthered because linear motion could be magnified with these devices. Two French scientists, Antoine-Laurent Lavoisier and Pierre-Simon Laplace, built the first dilatometer that provided accurate thermal expansion values in the late 1700s. The sample was a long rod and was submerged in a liquid bath at a known temperature. One end of the sample was in contact with a fixed vertical rod and the other end that was movable was attached to a lever that held a telescope. The telescope rotated in the vertical plane as the sample expanded and the coefficient of thermal expansion was given relative to the liquid bath housing material. The idea was eventually improved by using an optical lever in place of the telescope at the free end [15].

1.3.1.3 Modern Thermal Expansion Measurements

Various devices exist that can accurately measure thermal expansion. These are divided into basically two groups, namely comparators and levels, and are discussed briefly here.

A length comparator has two microscopes in fixed positions that can compare standards of lengths and small differences in lengths with the micrometer eyepieces. Precise temperature control is maintained by placing the sample in a liquid bath or a furnace to reach higher temperatures. Another method for thermal expansion measurements uses mechanical levers. A mechanical lever presses the sample flat against a micrometer screw. When the sample expands with temperature, it causes the lever to rotate which in turn, is measured by the screw. Pushrod dilatometers, like the one used in the thermal expansion measurements in this thesis, are abundant in laboratories for their accuracy and ease of use. The sample is placed in a tube and a rod rests against the sample. The tube and rod are usually made of fused silica. The sample end of the tube is placed in a furnace and expansion of the sample is measured by the displacement of the rod at the opposite end usually via a linear variable differential transformer (LVDT). Many more techniques are available for thermal expansion determination, but are mostly very advanced, such as interferometry and x-ray diffractometry. Moreover, the use of electrical parameters, such as capacitance and inductance can measure thermal expansion. An even more interesting method is the use of a volumetric dilatometer to measure a sample that is soft or exists only in the form of fine grains [15].

The abundance of thermal expansion measurements comes from the fact that there are so many ways to measure temperature and length. As mentioned, thermal expansion has been a wonder to scientists for centuries and they have worked to develop many different methods for

measuring it. It should be noted that most of the methods described are relative thermal expansion measurements and require calibration in the form of using reference materials.

1.3.1.4 Pushrod Dilatometers

As was discussed in the previous section, pushrod dilatometers facilitate the use of a rod that rests against the sample to transmit the small dimensional changes to the transducer. This is mainly because the electrical equipment cannot sustain the high temperatures involved in the thermal expansion measurements, so it must be insulated away from the sample [16]. The governing equations in the thermal expansion measurements are discussed later in the thesis, but it would be beneficial to discuss some of the components of pushrod dilatometers.

First, two tube orientations exist for pushrod dilatometers, namely horizontal and vertical. Horizontal dilatometers, like the one used in the experiments in this thesis, provide excellent uniform heating. However, vertical dilatometers do better with instances where shrinking occurs. In horizontal dilatometers, the force of the pushrod is increased to ensure that there is contact of the sample on the tube wall at all times. Nonetheless, both orientations have gained widespread use in laboratories [16].

The tube is closed at one end and the pushrod lays along the axis of the tube. The pushrod rests against the sample at the closed end of the tube. In the particular temperature range that was used for the experiments in this thesis, namely room temperature to 500°C, fused silica is used to make the tube and rod, mostly because of its low thermal expansion coefficient and stability. Other materials used at higher temperatures include alumina and graphite. A furnace encompasses the sample, pushrod, and tube. Most commonly, the furnace is made of a series of heating elements housed in an insulating container. A stable furnace response is

achieved through controllers that have an ideal heating rate. For example, the model used in the experiments recommends a heating rate of 3°C/minute. A thermocouple within the tube near the sample ensures this stable temperature response [16].

The process of converting the movement of the pushrod into a usable signal involves the use of transducers. Although there is more than one way to do this, the LVDT has become the primary choice for pushrod dilatometers. An LVDT consists of a cylindrical iron core that is wrapped by one primary and two secondary coils. The axial position of the core determines which secondary coil is better coupled with the primary coil, therefore producing a higher voltage. The signal is processed and recorded by the computer software. The transformer is lightweight and can be easily attached to the pushrod. However, it can have limitations if there is uneven winding of the coil and improper insulation [16].

1.3.1.5 Reference Materials and Sample Sizes

Alpha-alumina ($\alpha\text{-Al}_2\text{O}_3$) is the reference material supplied with the dilatometer that is used in the experiments. It is a readily available stable ceramic with a melting coefficient near 2027°C and a very low coefficient of thermal expansion. Other reference materials are copper, platinum, silica, silicon, tungsten, magnesium oxide, molybdenum, borosilicate glass, stainless steel, and graphite [17]. It is important that samples be of similar lengths to the reference material used for calibration in thermal expansion measurements. For example, the provided alumina sample was approximately 1” in length as was the Ti-N specimens that were provided for the experiments. However, 1” is not a nominal length for thermal expansion measurements since thermal expansion is not a property subject to size or shape. Samples should be stiff, though, and a rule of length-to-diameter of 4 to 1 is typically suggested. The intensive property

of thermal expansion allows for any shape of sample just as long as there is good contact with the closed end of the tube. Round samples as well as rectangular ones can be used since the cross-sectional area has no bearing on measurements. Samples must be representative of the entire material, though. This must be taken into consideration when experimenting with composites. Larger samples often bring with them the complications of temperature variations within the material. Also, these temperature gradients in the material can cause localized expansion and lead to errors. Moreover, testing time can be greatly increased with larger samples [16].

1.3.2 An Illustration: Al-1100-H14 versus Al-4032-T651

Increased nitrogen and oxygen in a material such as titanium increases brittleness and hardness in the material. The ultrasonic tests used in this thesis are very complicated measurements and become even more difficult because the titanium specimens tested are so small. To demonstrate the effect of increased hardness in a material, two aluminum alloys, namely Aluminum 1100-H14 and Aluminum 4032-T651, were tested. The specimens were 7” long, 1” wide, and 0.5” thick. Acousto-elastic and acousto-thermal tests were performed on these specimens and the goal was to attain differing acousto-elastic and acousto-thermal coefficients that could characterize the different aluminum alloys. Al-1100-H14 is commercially “pure” and Al-4032-T651 is an aluminum alloy of much higher hardness. Their compositions and material properties are listed below in Tables 1 and 2, respectively [18]:

Al-1100-H14		Al-4032-T651	
Component	Wt %	Component	Wt %
Al	Min 99	Al	81.1 – 87.2
Cu	0.05 - 0.2	Cr	Max 0.1
Mn	Max 0.05	Cu	0.5 - 1.3
Other, each	Max 0.05	Fe	Max 1.0
Other, total	Max 0.15	Mg	0.8 - 1.3
Si+Fe	Max 0.95	Ni	0.5 - 1.3
Zn	Max 0.1	Other, each	Max 0.05
		Other, total	Max 0.15
		Si	11 – 13.5
		Zn	Max 0.25

Table 1 Material compositions of Al-1100-H14 and Al-4032-T651.

	Al-1100-H14	Al-4032-T651
Brinell Hardness	32	120
σ_y	17 ksi	46 ksi
E	10,000 ksi	11,400 ksi
ν	0.33	0.34
$\alpha_{250^\circ\text{C}}$	14.2 $\mu\text{in/in-}^\circ\text{F}$	11.7 $\mu\text{in/in-}^\circ\text{F}$

Table 2 Material properties of Al-1100-H14 and Al-4032-T651.

σ_y is the yield stress in the material, E is the modulus of elasticity, ν is Poisson's ratio, and $\alpha_{250^\circ\text{C}}$ is the thermal expansion coefficient up to 250°C .

1.3.2.1 Acousto-Elastic Effect

A method of studying the nonlinear elastic behavior of materials is based on the so-called acousto-elastic effect. Acousto-elasticity is the stress-dependence of the acoustic velocity in a material [19]. The theory behind this effect is discussed later in the thesis, but it should be noted that the acousto-elastic effect can be demonstrated in any combination of propagation and polarization directions with respect to the direction of external stress. For a simple tensile stress case, there are five independent combinations of wave and polarization directions, namely longitudinal wave propagating parallel ($c_{d,p}$) and normal ($c_{d,n}$) to the external stress, a shear wave propagating parallel to the external stress ($c_{s,p}$), and two shear waves propagating normal to the external stress with either parallel ($c_{s,np}$) or normal ($c_{s,nn}$) polarization direction [19]. These combinations are shown in Figure 1. In this project, the evaluation of the acousto-elastic effect was limited to three polarizations for the same propagation direction, namely $c_{d,n}$, $c_{s,np}$, and $c_{s,nn}$, because of the limitation of the Material Test System (MTS).

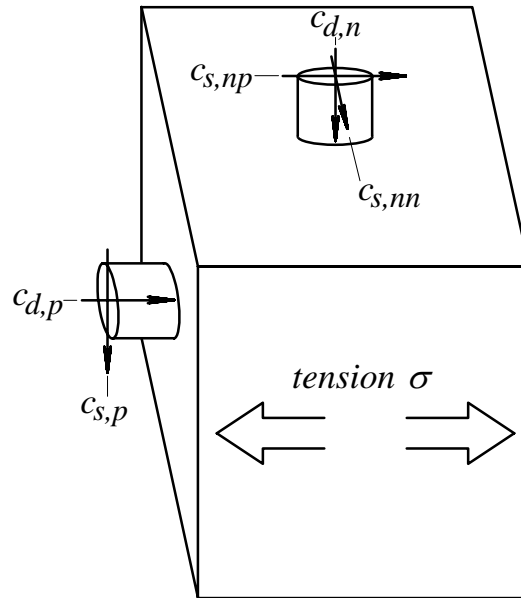


Figure 1 Principal directions of the acousto-elastic effect in isotropic materials [19].

The acousto-elastic effect is closely related to the thermal expansion coefficient and to the so-called acousto-thermal effect, or the temperature dependence of the sound velocity. These effects are rather small, but in general, the acousto-elastic effect and thermal expansion coefficient are relatively weaker than the acousto-thermal effect. The relative contributions of these phenomena are discussed later in the thesis.

The experimental setup and method of the acousto-elastic tests are discussed in detail later in the thesis, so it is not appropriate to repeat those details here. It is appropriate to mention some setup details of the experiments and then discuss the results. For Al-1100-H14, the scaling factor was set to 1,000 for longitudinal measurements and 5,000 for shear measurements. For Al-4032-T651, the scaling factor was set to 2,000 for longitudinal measurements and 10,000 for shear measurements. Moreover, for the Al-1100-H14 specimen, σ was varied from -5.6 to 5.6 ksi with a corresponding cross-sectional area of $S = 0.5 \text{ in}^2$, and σ was varied from -15.3 to 15.3

ksi with a corresponding cross-sectional area of $S = 0.5 \text{ in}^2$ for the Al-4032-T651 specimen. These stress ranges are one-third of the tensile yield strength of the material.

A common setback in the acousto-elastic measurements is drift in the signal due to temperature. The output of the Time Interval Counter (TIC) drifts with time due to temperature variations in the lab where the MTS is setup. Since the MTS program cycles 30 times, the drift has a dramatic impact on the output of the TIC. This temperature drift must be rectified in order to obtain a compact relative velocity change versus stress curve. First, each data point was averaged with the four points above and below it. Then, a periodic sampling of the data was taken to reduce the number of points by a factor of ten. This “new” set of points is representative of the larger set of points, but without the wide variation of points due to temperature drift. An example of temperature drift is shown in Figure 2. It shows a portion of the raw signal received by the MTS software versus time.

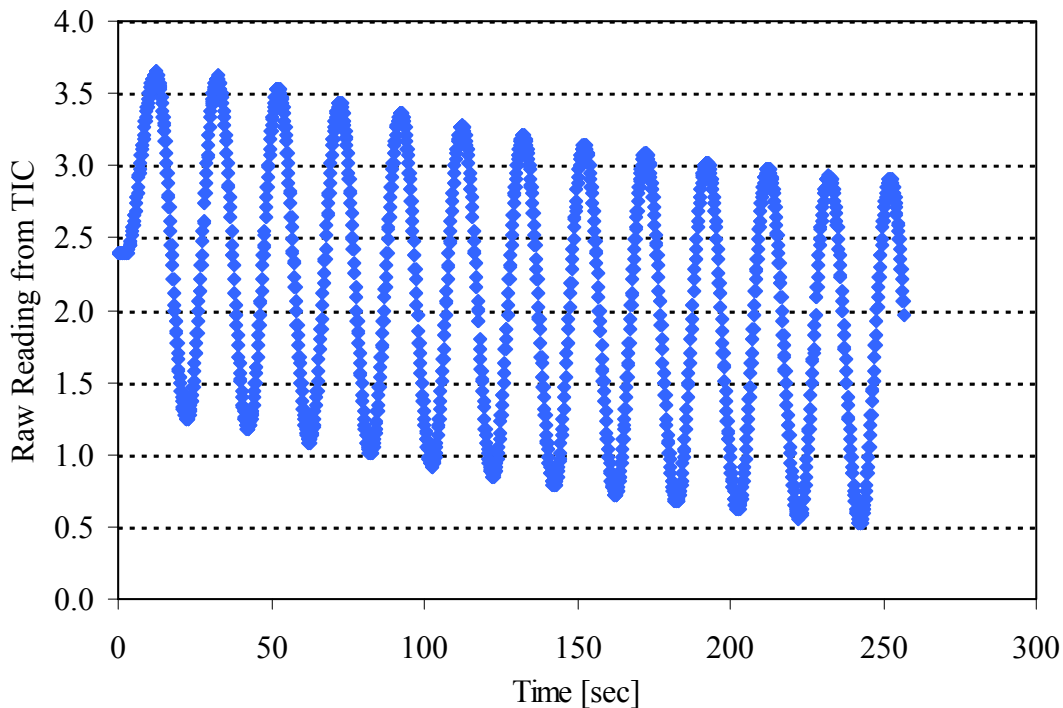


Figure 2 Reading from TIC versus time, showing drift of signal due to temperature fluctuations.

One way to eliminate drift is to isolate the specimen in an isothermal box. Many studies have been done to show the effects of temperature and stress on ultrasonic velocity. The goal of our acousto-elastic measurements was only to analyze the change in velocity with stress. It can also be shown through acousto-elastic experiments with well-controlled temperatures that the velocity change is proportional to the temperature change and, consequently, the acousto-elastic coefficient is directly related to this temperature change [20].

Our acousto-elastic measurements can be further complicated by other factors involving the transducer and couplant. Any slight misalignments of the transducer can cause errors in the signal read by the TIC. Furthermore, the honey used in the shear measurements as couplant hardens and sets after being applied to the transducer and may cause erroneous results if it is not given proper time to set. Moreover, the signal from the TIC must change a “sufficient” amount. This amount is related to the scaling factor described later and must be manipulated to obtain an optimum setting for a given material. These are various observed complications of the acousto-elastic measurements and they would only be magnified with much smaller specimens like the Ti-N specimens provided for this project.

Figures 3 and 4 show typical examples of the relative velocity change versus stress in Al-1100-H14 using a 0.5”-diameter, 5-MHz longitudinal transducer and a 0.5”-diameter, 5-MHz shear transducer at both normal and parallel polarizations. The slope of the graph of the relative velocity versus stress is the so-called acousto-elastic coefficient, K . The corresponding averaged acousto-elastic coefficients using a straight-line approximation are 5.7×10^{-5} , 17.3×10^{-5} , and $-21.2 \times 10^{-5} \text{ ksi}^{-1}$ for longitudinal and shear at normal and parallel polarizations, respectively.

Similarly, Figures 5 and 6 show typical examples of the relative velocity change versus stress in Al-4032-T651 using a 0.5”-diameter, 5-MHz longitudinal transducer and a 0.5”-

diameter, 5-MHz shear transducer at normal and parallel polarizations. The corresponding averaged acousto-elastic coefficients using a straight-line approximation are 4.8×10^{-5} , 9.8×10^{-5} , and $-13.3 \times 10^{-5} \text{ ksi}^{-1}$ for longitudinal wave and shear waves at normal and parallel polarization, respectively.

The results above show an approximate decrease in longitudinal and shear acousto-elastic coefficients of 15% and 60%, respectively, with increasing hardness. This means the harder, stronger Al-4032-T651 alloy has a lower acousto-elastic coefficient than the Al-1100-H14 alloy. This decrease is the same outcome as expected with the Ti-N samples. The nitrogen makes the titanium harder and should have a lower acousto-elastic coefficient.

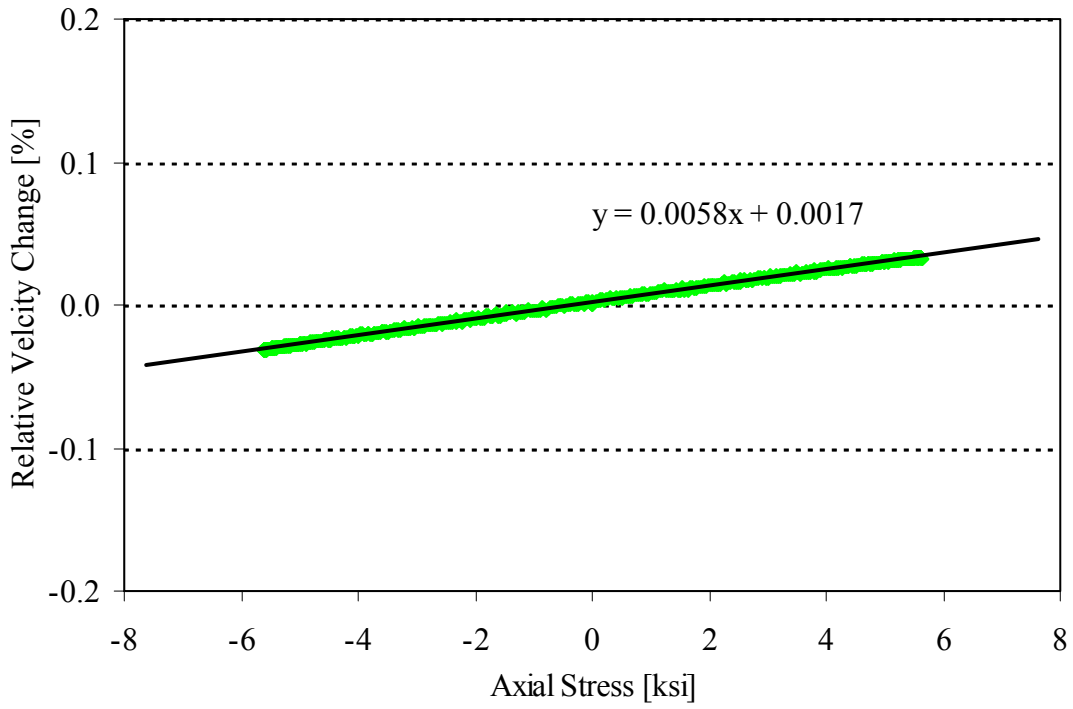


Figure 3 Relative velocity change versus stress in Al-1100-H14 using a longitudinal transducer.

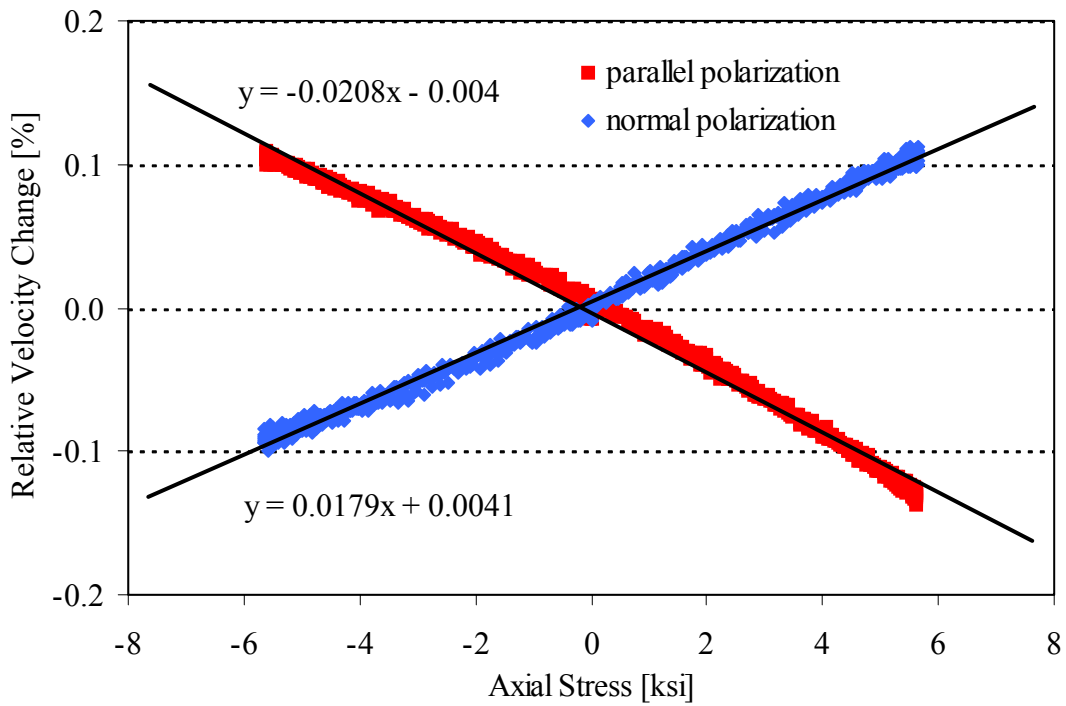


Figure 4 Relative velocity change versus stress in Al-1100-H14 using a shear transducer.

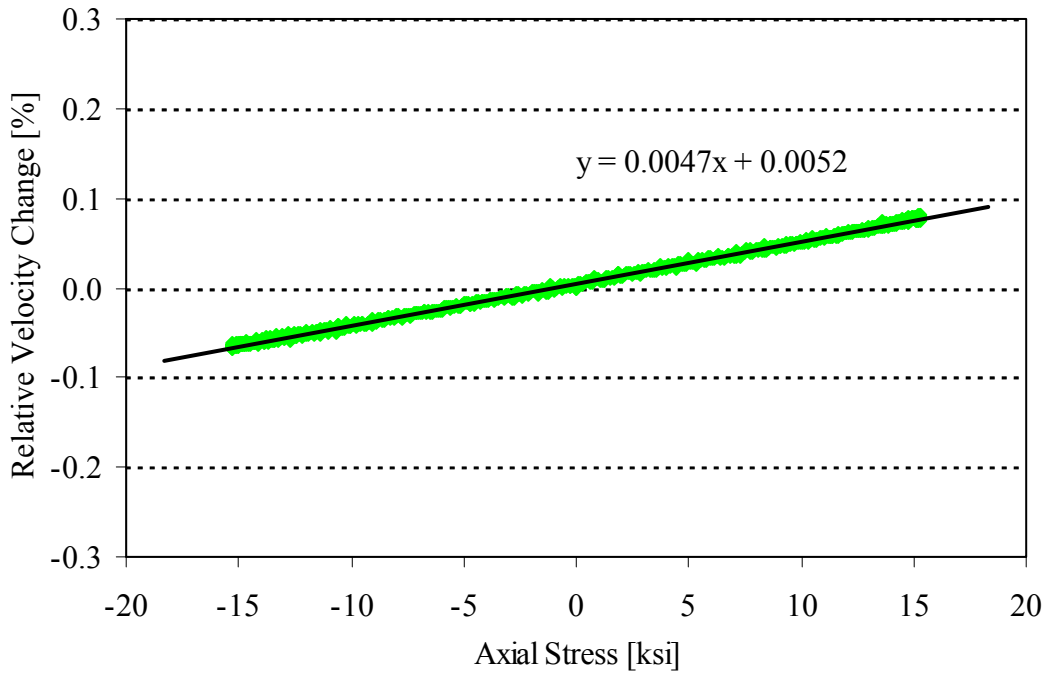


Figure 5 Relative velocity change versus stress in Al-4032-T651 using a longitudinal transducer.

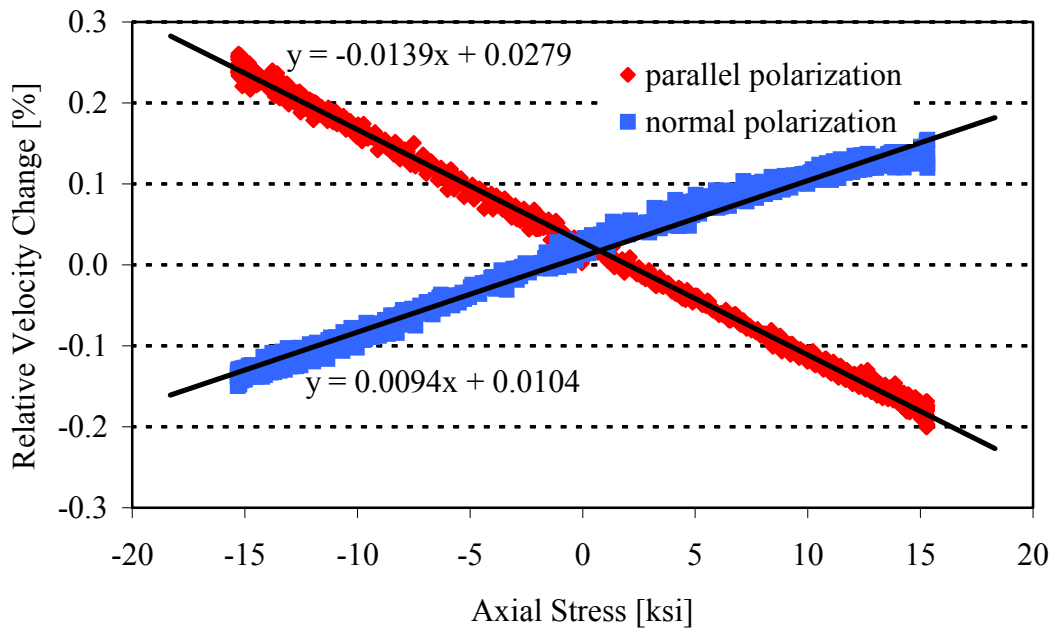


Figure 6 Relative velocity change versus stress in Al-4032-T651 using a shear transducer.

1.3.2.2 Acousto-Thermal Effect

The experimental setup and method of the acousto-thermal tests are discussed in detail later in the thesis, so it is not appropriate to repeat those details here. It is appropriate to mention some setup details of the experiments and then discuss the results.

The aluminum specimens were tested to see how the velocity in the specimen changed with temperature. The goal was to obtain three acceptable velocity versus temperature plots for each specimen using a 0.5"-diameter, 5 MHz longitudinal transducer.

Again, like the acousto-elastic measurement, the acousto-thermal measurement is very difficult. It is crucial to apply a thin layer of grease on the transducer to obtain reasonable results. Moreover, it is believed that the measurements are also affected by thermally aging transducers and microdot cables. Some of the tests performed on the aluminum specimens yielded erroneous results, namely the signal plotted in the Data Logger initially decreased with increasing temperature. This occurred for a very short period of time at the beginning of some tests. The signal eventually increased for the remainder of the heating period. This anomaly was attributed to the transducer and it was usually rectified in the next test by using a different transducer. However, a detailed study would need to be conducted on all of the variables of the acousto-thermal measurements to determine the cause of the erroneous results.

Figures 7 and 8 show typical examples of the apparent velocity versus temperature graph for Al-1100-H14 and Al-4032-T651, respectively. The averaged longitudinal acousto-thermal coefficients are -3.33×10^{-4} and $-3.31 \times 10^{-4}/^{\circ}\text{C}$ with standard deviations of 0.13 and 0.09 for Al-1100-H14 and Al-4032-T651, respectively.

The results show a slight decrease in increasing hardness, but it cannot be assumed from the standard deviations calculated. The accuracy could be increased with many more tests, but

the goal was only to show a brief illustration of the effect of hardness on the acousto-elastic and acousto-thermal coefficients and transfer these findings to the same tests performed on the Ti-N specimens. The results above do not show as significant a difference from Al-1100-H14 to Al-4032-T651 as was seen in the acousto-elastic measurements. These results also were somewhat hampered by experimental variables discussed above.

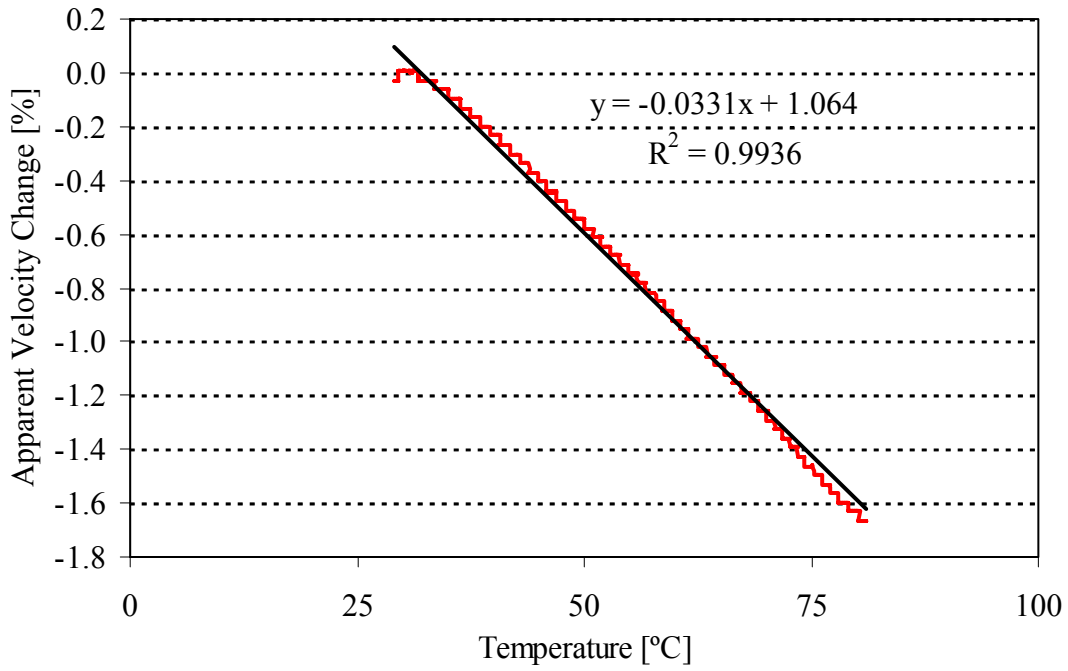


Figure 7 Apparent velocity change versus temperature in Al-1100-H14 using a longitudinal transducer.

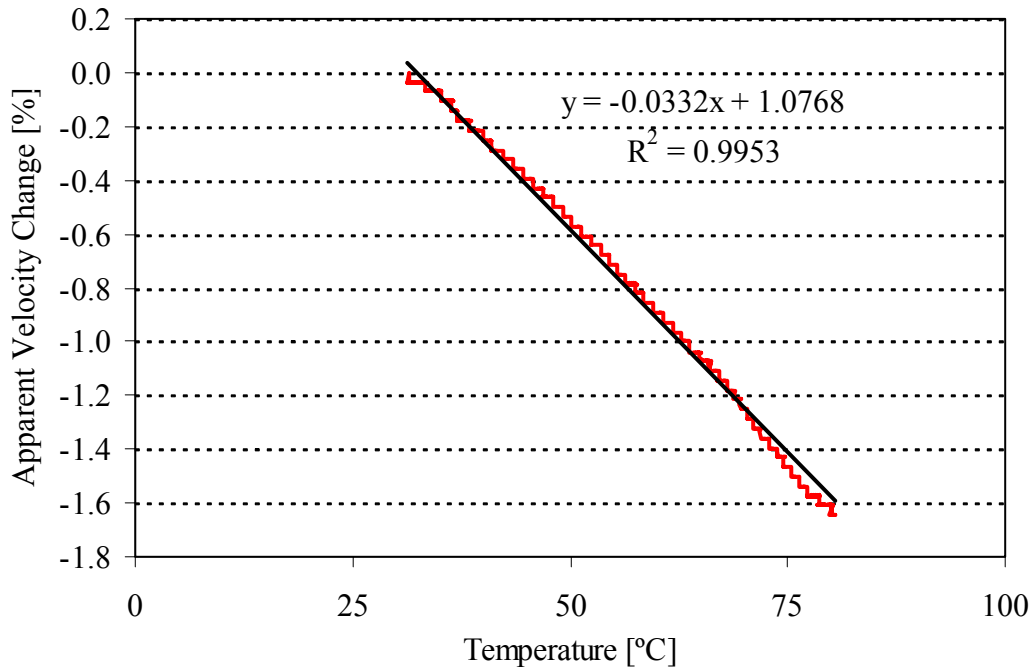


Figure 8 Apparent velocity change versus temperature in Al-4032-T651 using a longitudinal transducer.

2. Experimental Setup

2.1 Thermal Expansion Measurements

A schematic diagram and the experimental setup of the thermal expansion measurement are shown in Figures 9 and 10, respectively. The thermal expansion tests were done on an Orton Dilatometer Model 1600D. A dilatometer measures the so-called percent linear change (PLC) in a specimen by means of a Linear Variable Differential Transformer (LVDT) as it is heated by a furnace. This was discussed in detail in the introduction. The furnace can be heated to 1600°C in this particular model. A reference specimen made of alumina and a reference file was provided with the dilatometer equipment. A calibration run with the alumina specimen was made initially and compared with the reference values given by Orton so that accuracy of the dilatometer could be ensured. The calibration runs made by ourselves closely matched the reference plot provided by the company, but it was not exactly the same, therefore it was corrected so that future runs could be more accurate. Once the calibration run was completed, a calibration file was created with the necessary corrections and was used for all subsequent runs with other materials.

The accompanying software with the dilatometer made the experimental runs easy. The program includes a simple sheet with boxes clearly labeled to enter the specimen length, create a heating program, enter a file to save data, and specify which calibration file will be used. All runs started at room temperature and were heated at 3°C/minute to 500°C. Nominally the specimen lengths were 1” long. Once an experimental run was started, a graph showed the PLC versus temperature and the data was written to a user-created file. The information could then be imported into Excel to analyze further, namely to calculate the differential coefficient of

expansion (DOE) and the average coefficient of expansion (ACE), which is the value given in most textbooks.

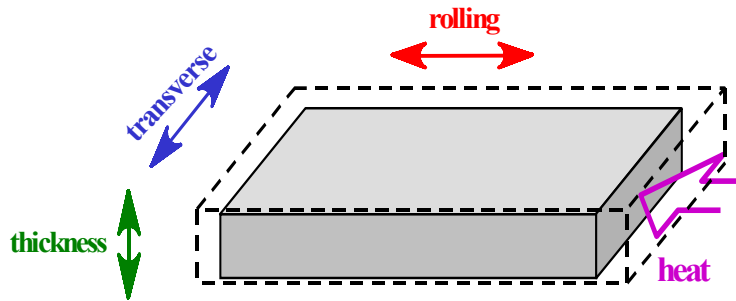


Figure 9 A schematic diagram of the thermal expansion measurements.

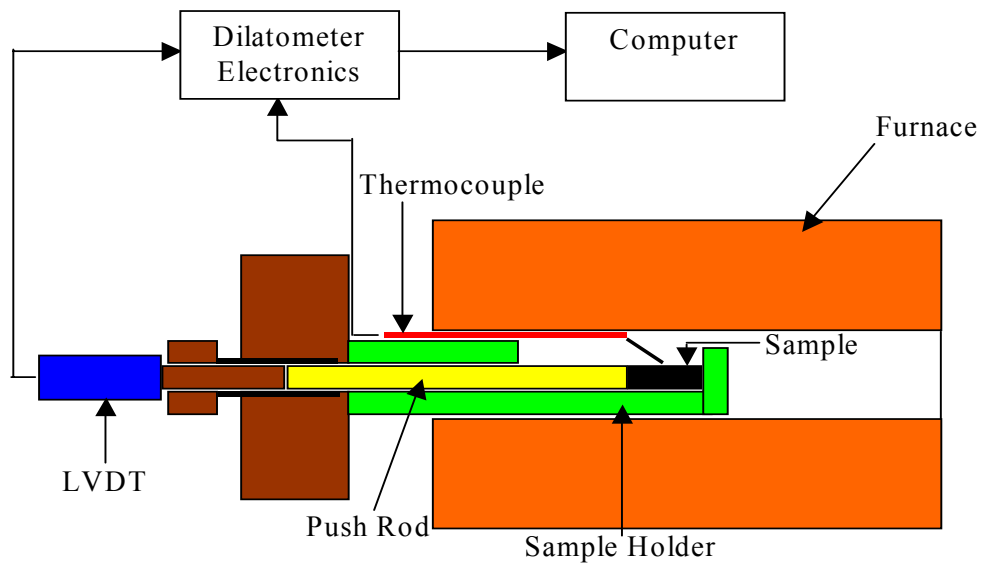


Figure 10 Experimental setup for thermal expansion measurements.

2.2 Acousto-Elastic Measurements

The goal of acousto-elastic measurements is to measure the relative velocity versus stress in a specimen. A schematic diagram of the direction of load from the MTS and the position of the transducer for longitudinal and shear measurements is shown in Figure 12. The experimental setup of the acousto-elastic measurement is shown in Figure 13. This is a very difficult measurement and requires some sophisticated equipment, namely a Stanford Research Systems, Inc. (SRS) Universal Time Interval Counter and an SRS Four-Channel Digital Delay/Pulse Generator, a Panametrics Pulser/Receiver, and a LeCroy Waverunner digital oscilloscope. The basic concept of this measurement is straightforward. First, a signal is created on the oscilloscope by means of the Pulser/Receiver and an appropriate transducer and couplant. For longitudinal measurements, a 0.25"-diameter, 5-MHz transducer was used with either grease or Vaseline as the couplant, and for shear measurements, a 0.25"-diameter, 5-MHz transducer was used with honey as the couplant. Then, with the Digital Delay/Pulse Generator, an "arming" gate is placed around the first two echoes from the specimen. This "arm" specifies the region in which the Time Interval Counter (TIC) measures the time delay. Appendix 1 lists the detailed setup parameters used in the time delay measurements. For accurate time measurement, one must choose to measure the corresponding positive or negative zero crossings on the first and second back wall echoes of the specimen. It is important to choose common points on each pulse to obtain an accurate reading. The details of setting the gate are shown in Figure 11. Points "P1" and "P2", shown in red on Figure 11, highlight the first positive zero crossings on the first and second back wall echoes, respectively. Points "N1" and "N2", shown in green on Figure 11, highlight the first negative zero crossings on the first and second back wall echoes, respectively. Both choices are acceptable and the "arming" gate must be placed in front of

points “P1” and “P2” or “N1” and “N2” for accurate time measurement. The “arming” gate, shown in pink in Figure 11, is optimized to measure the positive zero crossings (but could also work for the negative zero crossings).

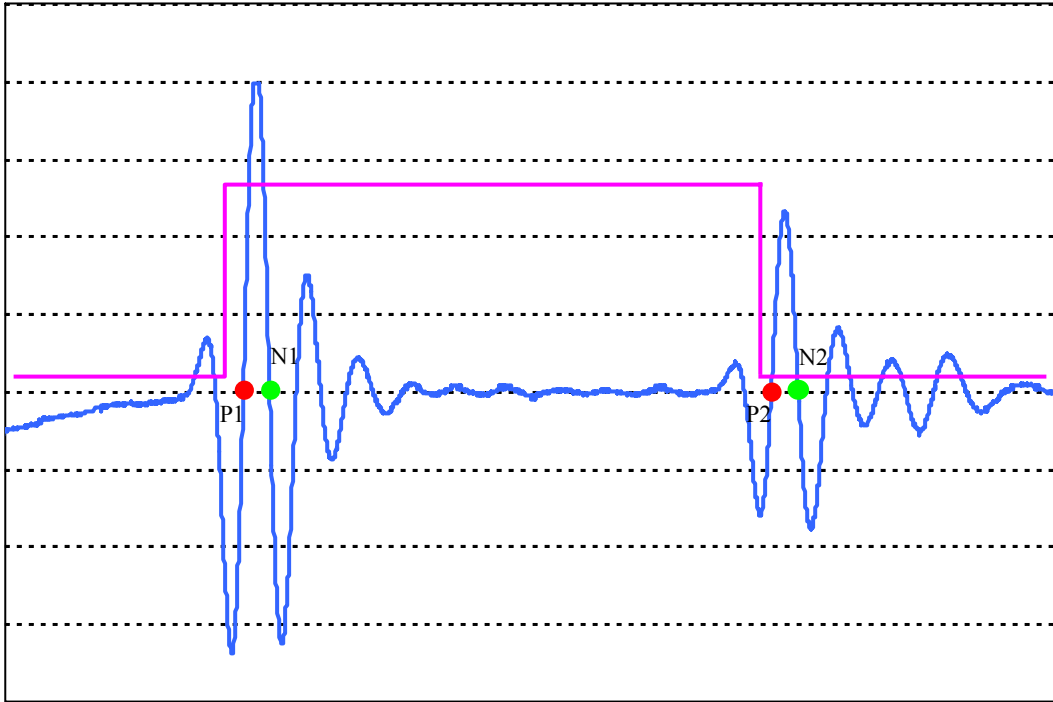


Figure 11 Explanation of positive and negative zero crossings to use for time measurements.

The MTS program, through Input Channel #1, reads the time delay from the D/A output marked “MEAN” on the TIC instrument. The “apparent” velocity can be determined directly from the measured propagation time delay and the nominal thickness of the specimen. In order to determine the actual sound velocity, the thickness of the specimen must be corrected for changes due to the so-called Poisson effect.

Once a good signal was established, the specimen was placed in the Material Test System (MTS) and set in place. This meant gripping both ends of the specimen while the transducer was

clamped somewhere in the middle of the specimen. A simple program was created on the MTS software for the acousto-elastic measurements. This program dwells for two seconds, then cycles at 0.05 Hz for 30 cycles at a stress level of one-third of the nominal yield stress of the material. During the experiment, the axial force and the two-way propagation time delay from the Time Interval Counter is plotted against time. When the cycles are completed, the force is ramped to zero and the program is complete. The complete data set, namely a time stamp, the axial force from the MTS, and the two-way propagation time from the TIC, was written to a file, which could be imported into an Excel spreadsheet for analysis.

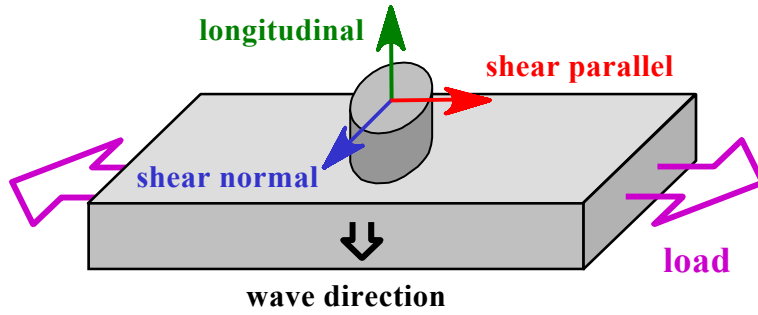


Figure 12 A schematic diagram of the acousto-elastic measurements.

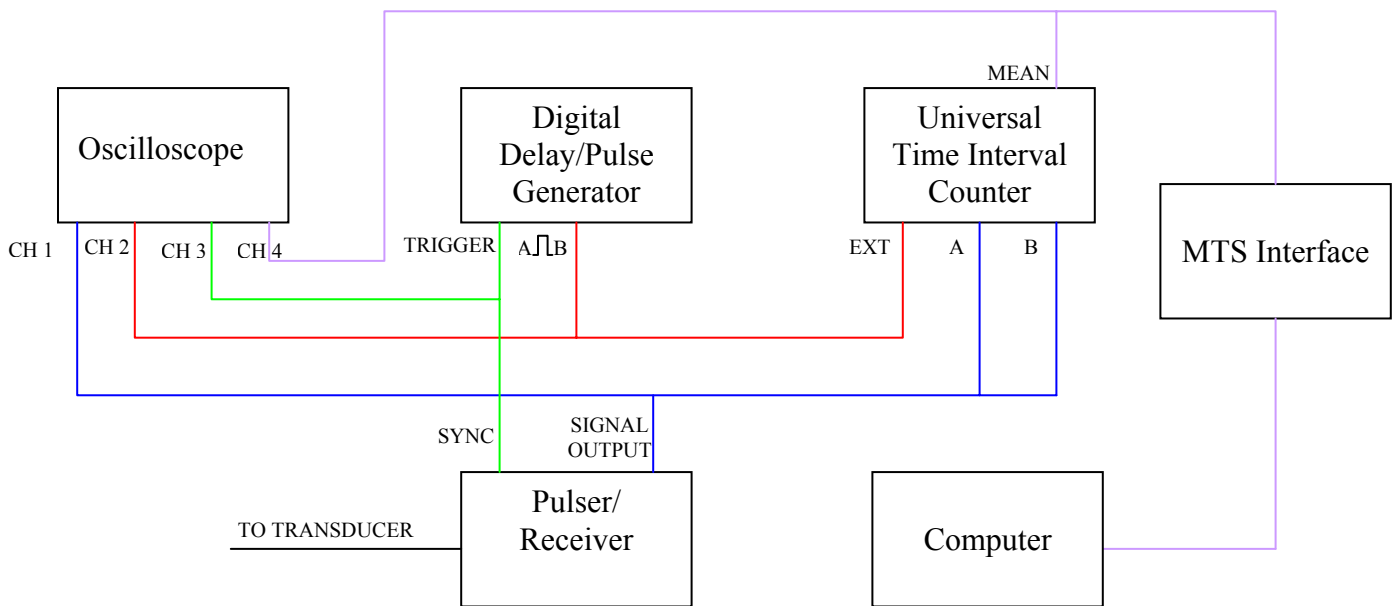


Figure 13 Experimental setup for acousto-elastic measurements.

2.3 Acousto-Thermal Measurements

The goal of acousto-thermal measurements is to measure the relative velocity versus temperature in a specimen. A schematic diagram and the experimental setup of the acousto-thermal measurement are shown in Figures 14 and 15, respectively. This is also a very complicated measurement like the previously described acousto-elastic measurement. As can be expected, the same equipment is used to measure the time delay in the specimen, which in turn is used to calculate the velocity. However, instead of stressing the specimen in the MTS, the specimen was placed in a water bath in a Pyrex dish and subjected to temperature variations. 5-MHz longitudinal and shear transducers were used in the acousto-thermal measurements. The transducer was placed on one side of the specimen and a bracket was placed on the other side of the specimen with everything clamped together and placed in the water. The bracket is U-shaped and provides a gap on the underside of the specimen where the transducer signal acts.

An identical reference specimen with a Type K thermocouple mounted on it was also placed in the bath to measure the temperature. For the longitudinal measurements, the glass dish was then placed on a Dataplate Digital Hot Plate to be heated. The temperature range used in these experiments was from room temperature to 80°C. The water bath was let cool back to room temperature after the initial heating was finished. The cooling part of the temperature profile was slower and more reproducible, therefore the acousto-thermal coefficient was measured in that range. The propagation time delay increases as the temperature increases and decreases as the temperature decreases and this was recorded by use of a Virtual Bench Data Logger that is part of Labview. A connection was made to the D/A Output marked “MEAN” of the Stanford Time Interval Counter and passed to an A/D board. The thermocouple was also connected via a preamplifier to the A/D board to be relayed to the computer and displayed and

written to a file by the Data Logger. The Data Logger displayed the temperature of the reference specimen and the two-way propagation time delay versus time. The only difference with the shear measurements was in the method of heating and cooling. The longitudinal wave couplant used was grease and although it probably lost some of its viscosity when heated, it did not affect the measurements. Shear wave couplants lose their needed high viscosity at higher temperatures and therefore the signal slowly decays on the oscilloscope. Eventually, the signal disappears completely, typically around 55-60°C. In addition to decreased viscosity, honey dissolves in water and cannot be used for the thermal measurements, therefore a special Panametrics shear wave couplant was used in these experiments. Instead of heating on the hot plate, a Neslab chiller was used to extend the temperature range, since the chiller can both heat and cool the water. The temperature was first increased from room temperature to 45°C, then cooled to 5°C. This range is broader by approximately 15°C than what would be achievable using the hot plate since the hot plate would only allow the specimen to be heated to 45°C, then cooled to room temperature.

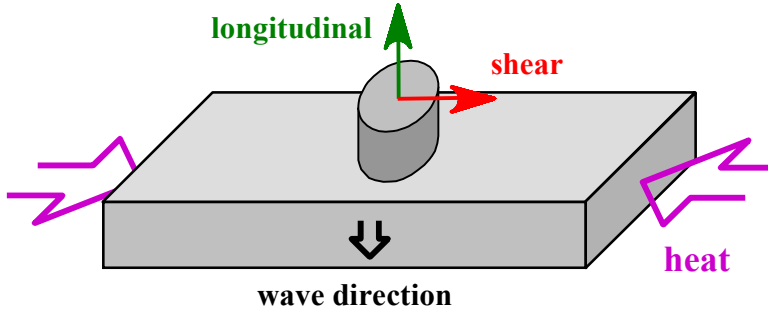


Figure 14 A schematic diagram of the acousto-thermal measurements.

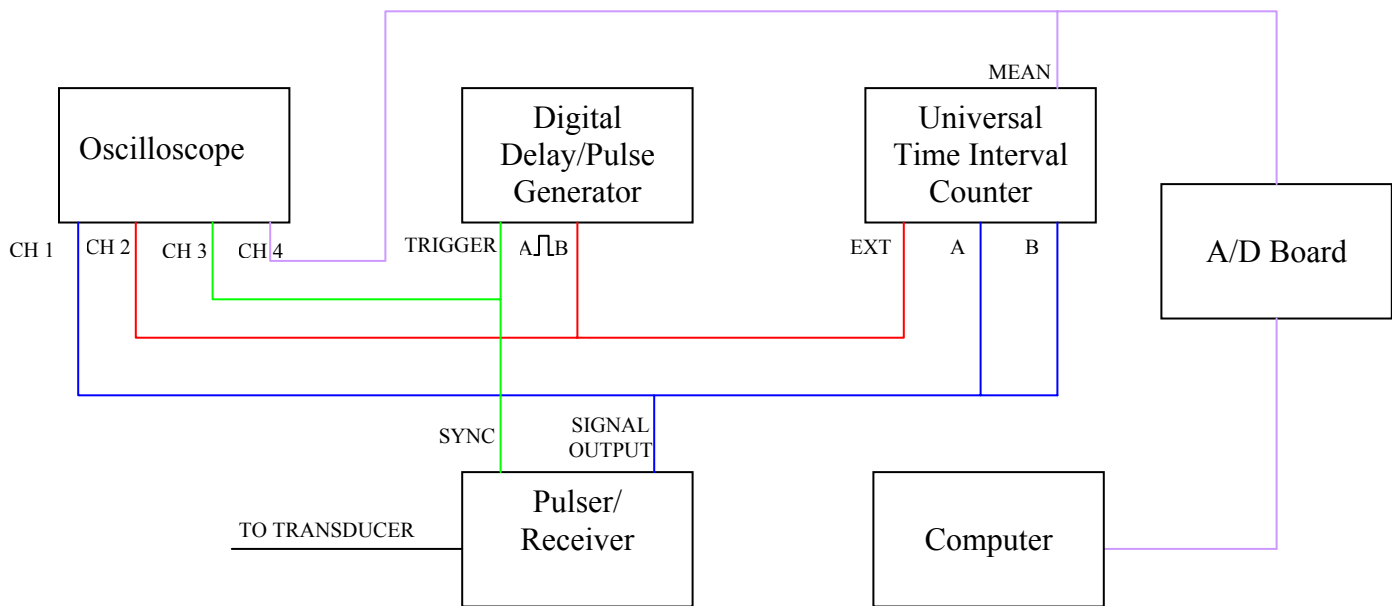


Figure 15 Experimental setup for acousto-thermal measurements.

3. Results

3.1 Thermal Expansion Coefficient

Materials can be characterized by a thermal expansion coefficient that measures how much the material expands over a certain temperature range. This parameter is mostly used to compare materials, shown as the average coefficient of expansion (ACE) below, but other parameters can be calculated as well, including the percent linear change (PLC) and the differential coefficient of expansion (DCE). The ACE is of the most interest in the experiments conducted in this study. The PLC is the percentage that the specimen expanded from its original length, or

$$PLC = \frac{l_T - l_0}{l_0} \times 100, \quad (1)$$

where l_0 is the original length of the specimen and l_T is the length of the specimen at the final temperature. The DCE is the amount the specimen expanded from its original length over a twenty-degree temperature range

$$DCE = \frac{(l_T - l_{T-20})/l_0}{20}, \quad (2)$$

where l_{T-20} is the length at twenty degrees below the final temperature. Finally, the ACE is the amount the specimen expanded from its original length over the entire temperature range of the experiment

$$ACE = \frac{(l_T - l_0)/l_0}{T - T_0}, \quad (3)$$

where T is the final temperature and T_0 is the initial temperature. The experiments performed in this study compared pure titanium and Ti-6Al-4V titanium alloy with no nitrogen content to titanium with varying levels of nitrogen content from 2.5% to 5.9%.

Several practice runs were made with the dilatometer using Ti-6Al-4V specimens. The object was to obtain results similar to the accepted thermal expansion coefficient for this common titanium alloy, namely $\alpha_{\text{Ti-6Al-4V}} \approx 8.6 \times 10^{-6}/^{\circ}\text{C}$ to $9.7 \times 10^{-6}/^{\circ}\text{C}$ between 20°C and 500 °C [18]. An extensive study was done on textured Ti-6Al-4V and the results were comparable to the above values. Six specimens were machined from a large piece of forged Ti-6Al-4V. Two pieces were machined in each of the axial, transverse, and vertical directions, namely the typical x , y , and z coordinate directions. Experimental runs were performed on these specimens and the average coefficient of expansion for each orientation was calculated. The results listed in Table 3 are comparable to the accepted expansion coefficient of Ti-6AL-4V and it was determined that the dilatometer was giving accurate results.

At 500°C	Axial Trial #1	Axial Trial #2	Transverse Trial #1	Transverse Trial #2	Vertical Trial #1	Vertical Trial #2
PLC [%]	0.439	0.449	0.453	0.435	0.450	0.412
ACE [$10^{-6}/^{\circ}\text{C}$]	9.39	9.58	9.68	9.30	9.67	8.85

Table 3 PLC and ACE of Ti-6Al-4V directional (textured) specimens.

The next step was to test the Ti-N specimens provided by MLLP/AFRL. These were titanium specimens of varying nitrogen content, namely 2.5%, 3.1%, 3.8%, 4.8%, and 5.9% nitrogen. Also provided by Honeywell Engines was a titanium billet specimen with no nitrogen content, and canted and forged Ti-6Al-4V specimens. Four experimental runs were performed and the averaged results are listed in Table 4.

Figures 16 and 17 show the PLC and ACE versus temperature curves of one of the four trials. Table 4 shows that the PLC and ACE both decrease with increasing levels of nitrogen. This is to be expected since nitrogen makes titanium more brittle and brittle materials do not

expand as much as more ductile materials, like pure titanium with no nitrogen content. However, as will be shown in a following section, the relative contribution of this observed dimensional change to the overall temperature effect is very small.

At 500°C	2.5% N	3.1% N	3.8% N	4.8% N	5.9% N	Billet	Canted	Forged
PLC [%]	0.386	0.381	0.365	0.331	0.321	0.439	0.438	0.439
ACE [$10^{-6}/^{\circ}\text{C}$]	8.29	8.19	7.81	7.08	6.88	9.41	9.39	9.41

Table 4 PLC and ACE of titanium specimens with varying levels of nitrogen.

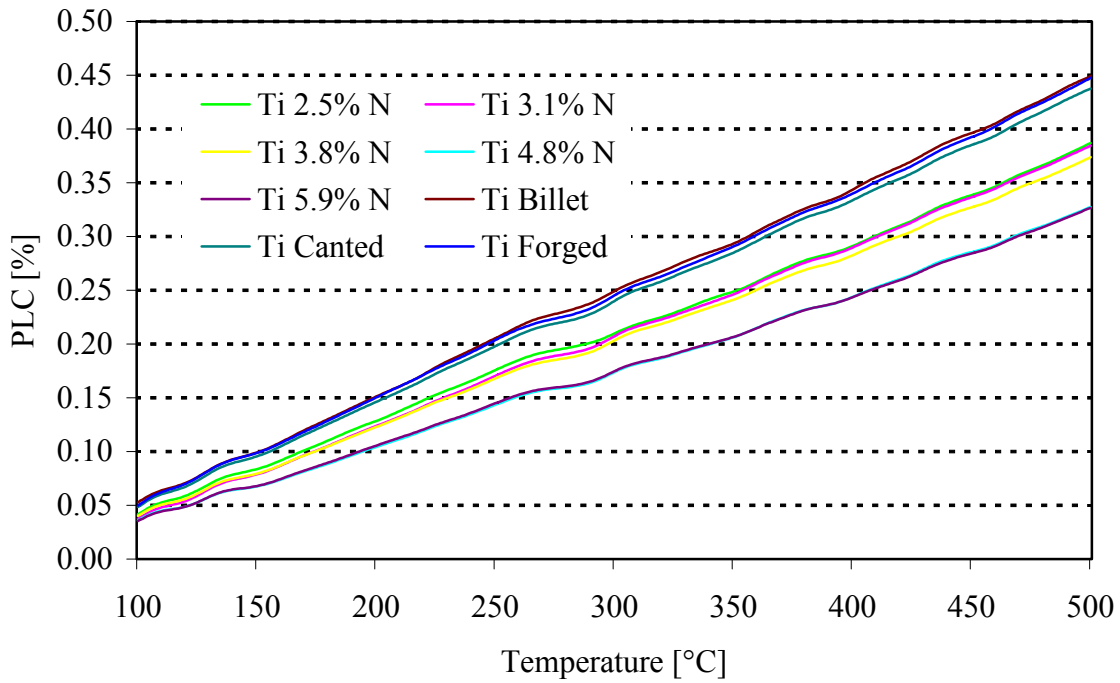


Figure 16 PLC versus temperature for titanium with varying levels of nitrogen content.

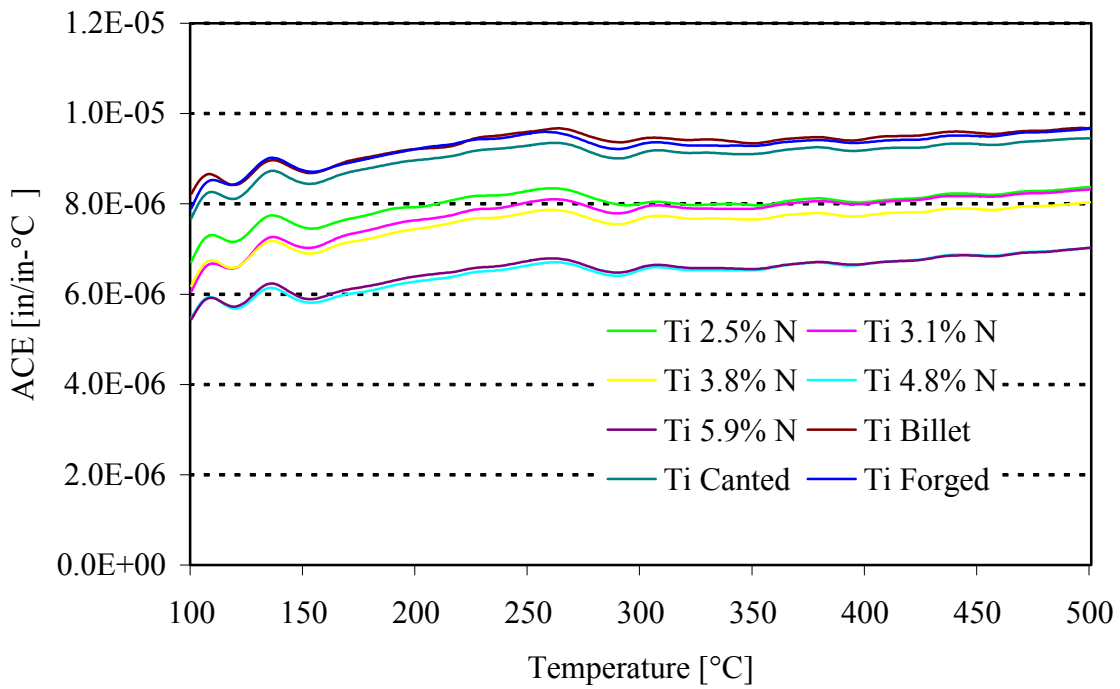


Figure 17 ACE versus temperature for titanium with varying levels of nitrogen content.

3.2 Acousto-Elastic Coefficient

The acousto-elastic measurement was the most difficult of the three measurements. Since the nitrogen-enriched specimens were very small and weakened by both embrittlement and micro-porosity, they could not be tested in the MTS machine for fear of ruining them. In addition, the grips of our 100-kN MTS machine could not be adapted to hold these small pieces, therefore the specimen would have to be tested in compression with a high risk of buckling failure. Thus, since the variations in the acousto-elastic effect are expected to play a minimal role in the detectability of hard-alpha inclusions, only baseline measurements were made in Ti-6Al-4V reference specimens without jeopardizing the small, embrittled Ti-N specimens.

First, a piece of Al-2024 was tested since the acousto-elastic coefficient was already measured in the same specimen previously [21]. Then, a rolled piece of Ti-6Al-4V was tested in the same manner. The goal was to gather some baseline data on the acousto-elastic coefficients and estimate the order of magnitude of the maximum relative change in velocity that could be seen in the presence of thermal stresses. Both longitudinal and shear transducers were used in these measurements. Data acquisition was controlled by the MTS program described earlier. A shear transducer was also used at normal and parallel polarization, meaning the particle displacements were aligned normal and parallel to the direction of the unidirectional stress, respectively. The crucial part of the measurements was to measure the relative change of the instantaneous time delay by the Time Interval Counter (TIC). The initial time delay was recorded before the MTS program was started and then the “Set Rel(ative)” button on the Time Interval Counter was pressed so that the measurements would be taken relative to this initial time delay. Also recorded through the MTS data acquisition system were the voltages at the initial time delay and when it was zeroed at the start of the measurement for subsequent calibration of

the analog output signal of the TIC. The time, applied force, and analog output from the TIC were written to a file as the program ran.

Also very important for the measurement is the scaling factor on the TIC. The scaling factor is a measure of how much the input signal to the computer, i.e., the analog output of the TIC, changes for a given change in time delay. The scaling factor had to be adjusted on a case-to-case basis to avoid saturating the output signal from the TIC. The available signal is from 0-8 V and the scaling factor was increased for shear measurements since the relative increase in the time delay was greater than in the longitudinal measurements. For Al-2024, the scaling factor was set to 5,000 for longitudinal measurements and 10,000 for shear measurements. For Ti-6Al-4V, the scaling factor was set to 2,000 for longitudinal measurements and 5,000 for shear measurements.

Once the data was imported into Excel, the relative velocity was calculated. First, from the time delays that were recorded before the program started, relative change in the two-way propagation time $\Delta t/t_0$ was calculated from

$$\frac{\Delta t}{t_0} = \frac{A(V - V_0)}{t_0}, \quad (4)$$

where A [$\mu\text{s}/\text{V}$] is the measured slope associated with the scaling factor, V [V] is the analog output of the TIC recorded by the computer as the specimen is stressed and written to file, V_0 [V] is the analog output of the TIC recorded once the “Set Rel” button was pressed, and t_0 [μs] is the initial time delay recorded by the operator from the Time Interval Counter.

The measured slope is a value dependent on the scaling factor. It was calculated by first obtaining a signal on the oscilloscope with a transducer using a generic specimen. Then, the “Set Rel” button was pressed. The relative value on the Time Interval Counter and the corresponding

voltage on the MTS were then recorded several times. Next, the transducer was moved to a different spot on the specimen, where the thickness was inevitably slightly different, and the procedure was repeated. In this way, a well-controlled time delay could be simulated for calibration purposes. Then, the averaged time delays at both transducer locations from the Time Interval Counter were subtracted. The same procedure was followed for the average values of the voltages recorded by the A/D converter. The results were finally divided to obtain a slope in $\mu\text{s}/\text{V}$. In this way, the entire data acquisition system could be accurately calibrated without separately calibrating each elements of the system.

The Poisson correction was then made to account for the changing cross-sectional area as the specimen was put in tension and compression. The lateral strain is given by

$$\frac{\Delta d}{d_0} = -\frac{\sigma \nu}{E} \quad (5)$$

where σ is the applied stress, ν is Poisson's ratio in the material, and E is the modulus of elasticity. For Al-2024, σ was varied from -15 to 15 ksi with a corresponding cross-sectional area of $S = 0.5 \text{ in}^2$, $\nu = 0.33$, and $E = 10,700$ ksi. For Ti-6Al-4V, σ was varied from -30 to 30 ksi with a corresponding cross-sectional area of $S = 0.203 \text{ in}^2$, $\nu = 0.33$, and $E = 16,500$ ksi. Without the Poisson correction, the slope of the relative velocity versus stress curve is larger than with the correction since some of the apparent velocity change is due to the Poisson effect. Using the correction yields a more accurate acousto-elastic coefficient. Finally, the relative velocity change is the Poisson correction minus $\Delta t/t_0$, or

$$\left. \frac{\Delta c}{c_0} \right|_{\text{AE}} = -\frac{\sigma \nu}{E} - \frac{\Delta t}{t_0} \quad (6)$$

Figures 18 and 19 show typical examples of the relative velocity versus stress in Al-2024 using a 0.25"-diameter, 5-MHz longitudinal transducer and a 0.25"-diameter, 5-MHz shear transducer at both normal and parallel polarizations. The slope of the graph of the relative velocity versus stress is the so-called acousto-elastic coefficient, K . The corresponding averaged acousto-elastic coefficients using a straight-line approximation are 6.2×10^{-5} , 6.4×10^{-5} , and $-15.3 \times 10^{-5} \text{ ksi}^{-1}$ for longitudinal and shear at normal and parallel polarizations, respectively. These values are in reasonable agreement with previously published results [21].

Similarly, Figures 20 and 21 show typical examples of the relative velocity versus stress in Ti-6Al-4V using a 0.25"-diameter, 5-MHz longitudinal transducer and a 0.25"-diameter, 5-MHz shear transducer at normal and parallel polarizations. The corresponding averaged acousto-elastic coefficients using a straight-line approximation are 1.4×10^{-5} , 7×10^{-5} , and $-11.5 \times 10^{-5} \text{ ksi}^{-1}$ for longitudinal wave and shear waves at normal and parallel polarization, respectively.

As can be seen, the acousto-elastic coefficients are very small because the relative velocity only changes merely 1% at stress levels as high as the yield strength of the material. It would be possible to test the effect of nitrogen in titanium with either larger specimens or at lower levels of applied stress, but the evaluation of the data would be susceptible to large errors because of the small change in relative velocity. Utilizing a larger stress range would be dangerous, too, because there would be a risk of breaking the specimens.

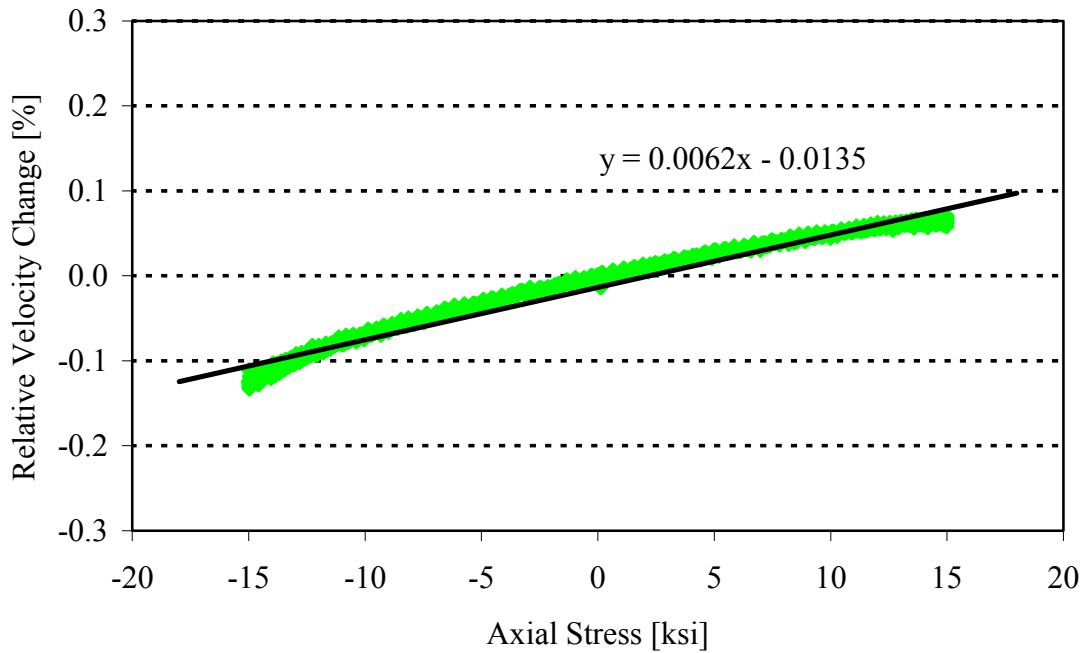


Figure 18 Relative velocity change versus stress in Al-2024 using a longitudinal transducer.

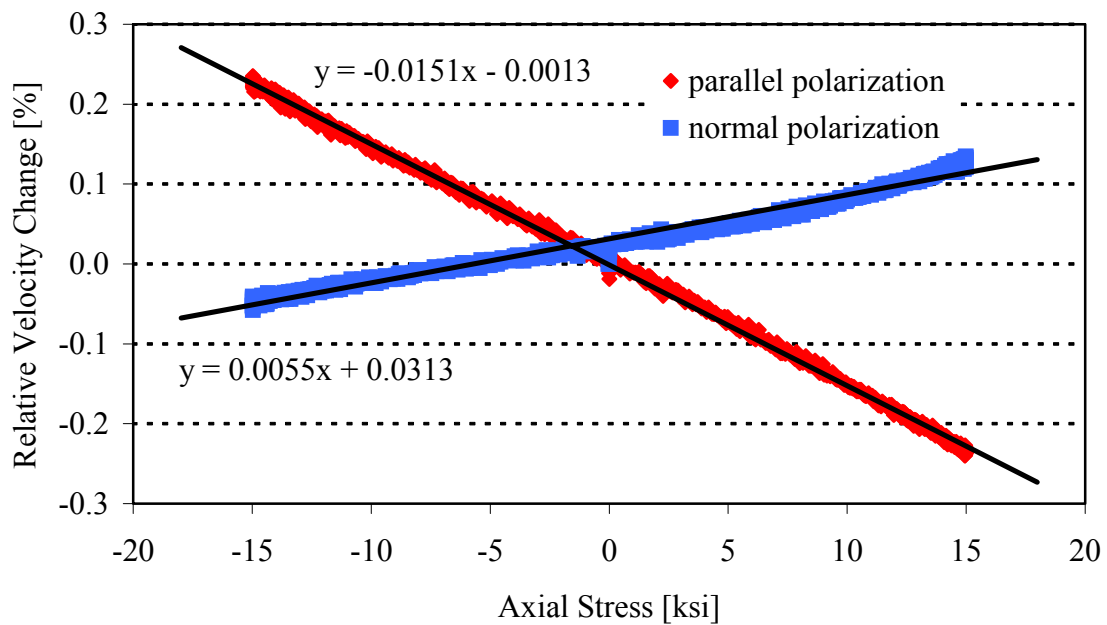


Figure 19 Relative velocity change versus stress in Al-2024 using a shear transducer.

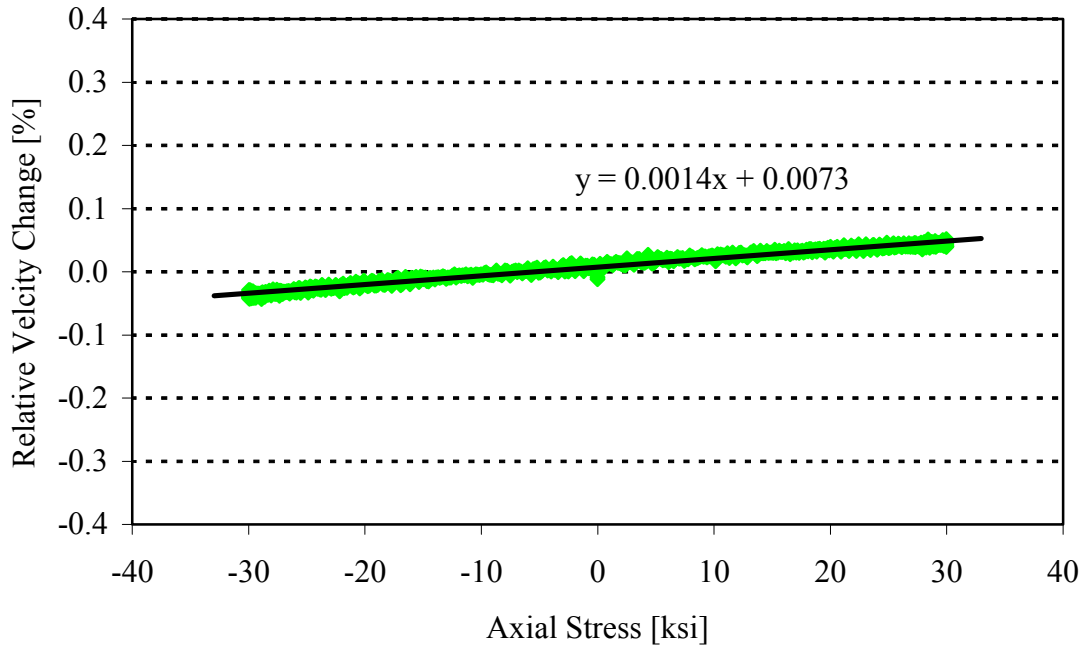


Figure 20 Relative velocity change versus stress in Ti-6Al-4V using a longitudinal transducer.

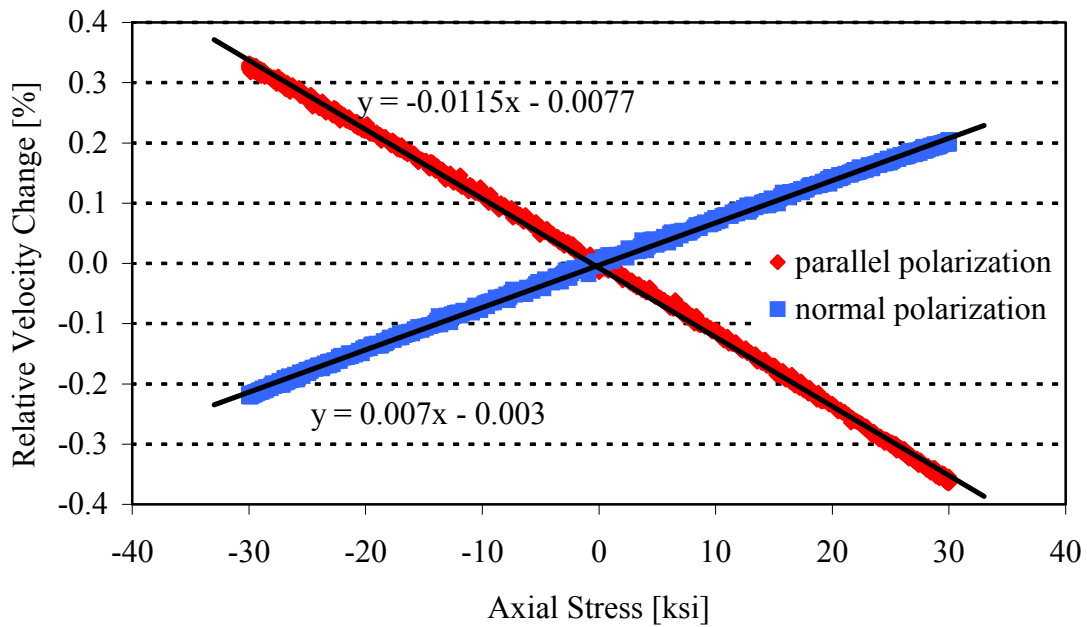


Figure 21 Relative velocity change versus stress in Ti-6Al-4V using a shear transducer.

3.3 Acousto-Thermal Coefficient

The acousto-thermal measurement is very similar to the acousto-elastic measurement in that the same equipment is used to measure the time delay. The calculation of the relative velocity was somewhat simpler than discussed above because, for simplicity, only the apparent velocity was analyzed without correcting for the changing propagation length due to thermal expansion, i.e., the apparent velocity change includes a small part due to changes in dimension. Once the data was imported into Excel from the Data Logger, the apparent relative velocity change was calculated from

$$\frac{\Delta c_{\text{apparent}}}{c_0} = - \frac{\Delta t}{t_0} = - \frac{A \Delta V}{t_0} \quad (7)$$

where, as before, A [$\mu\text{s}/\text{V}$] is the measured slope associated with the scaling factor, the ΔV [V] is the change in the analog output signal from the Time Interval Counter (TIC), and t_0 [μs] is the initial time delay recorded by the operator on the TIC.

Among the specimens that were tested titanium grade 2 and rolled Ti-6Al-4V were included. These specimens were only tested for a better comparison in addition to the specimens from Honeywell. Each specimen had an identical counterpart to be used as the reference for temperature measurements so that electrical grounding problems could be avoided. The specimens provided by Honeywell Engines, namely a forged Ti-6Al-4V specimen and a titanium billet specimen, as well as the 2.5% N, 3.1% N, and 3.8% N titanium specimens from AFRL, were also tested in the same way. The Ti-6Al-4V canted specimen was used as the reference specimen when testing these specimens. The goal was to obtain six acceptable velocity versus temperature plots for each specimen using both longitudinal and shear wave transducers. In order to limit gross measurement errors, acceptable experimental data was defined as a curve

with a linear regression of $R^2 = 0.95$ or better. This acousto-thermal test is a very complicated one and it becomes excessively difficult with the smaller specimens. Many factors can easily hinder the experiment, namely the amount of couplant on the transducer, the water level in the bath, or even a degenerating (thermally aging) transducer or microdot cable. Therefore, the R^2 criterion was imposed so as to accept only sufficiently linear velocity versus temperature curves. Tables 5 and 6 list the averaged acousto-thermal coefficients of the tested specimens and the corresponding standard deviations for longitudinal and shear waves, respectively.

	Acousto-Thermal Coefficient [$10^{-4}/^{\circ}\text{C}$]						
	Titanium	Ti-6Al-4V	Forged	Billet	2.5% N	3.1% N	3.8% N
Average	-2.41	-2.35	-2.10	-1.92	-2.32	-1.86	-1.20
Std. Dev.	0.10	0.28	0.19	0.47	0.25	0.42	0.16

Table 5 Measured acousto-thermal coefficients using a 5-MHz longitudinal transducer

	Acousto-Thermal Coefficient [$10^{-4}/^{\circ}\text{C}$]						
	Titanium	Ti-6Al-4V	Forged	Billet	2.5% N	3.1% N	3.8% N
Average	-6.86	-8.94	-7.28	-7.65	-7.02	-8.38	-12.86
Std. Dev.	0.44	0.61	0.28	0.33	0.53	0.45	0.48

Table 6 Measured average acousto-thermal coefficient using a 5-MHz shear transducer.

In order to illustrate the actual raw data used to obtain the results listed in Tables 5, Figures 22 and 23 show two measured velocity versus temperature graphs for the 3.1% TiN specimen. Figure 22 shows an acceptable curve of $R^2 = 0.996$ whereas Figure 23 shows a curve of $R^2 = 0.919$ that was determined to be unacceptable because of its excessive nonlinearity.

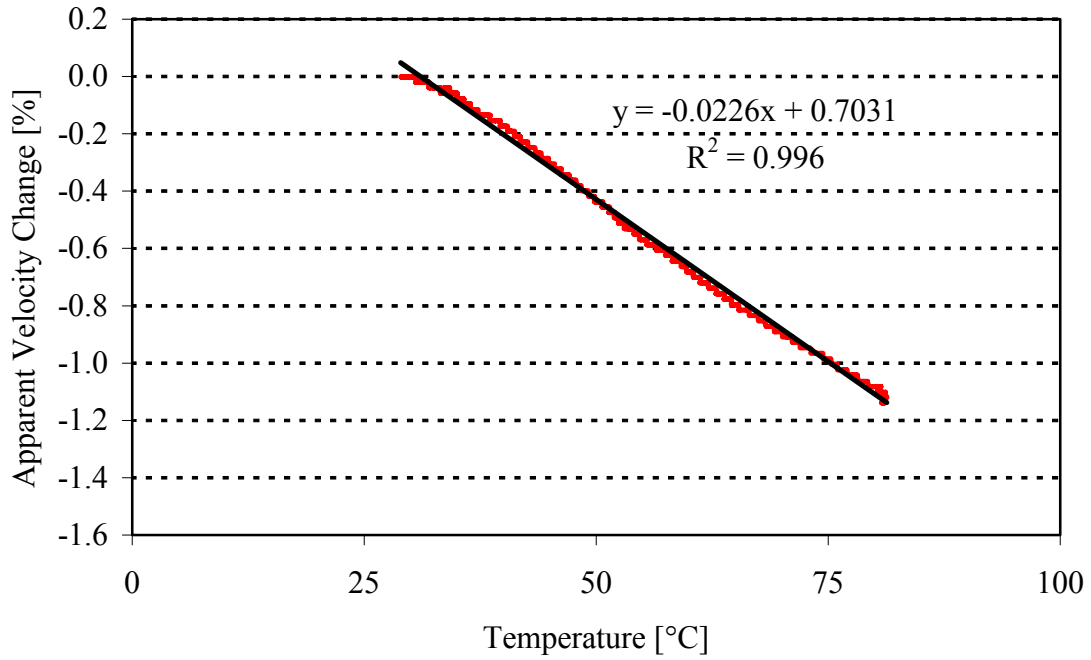


Figure 22 Apparent velocity change versus temperature in titanium with 3.1% N using a longitudinal transducer (acceptable data).

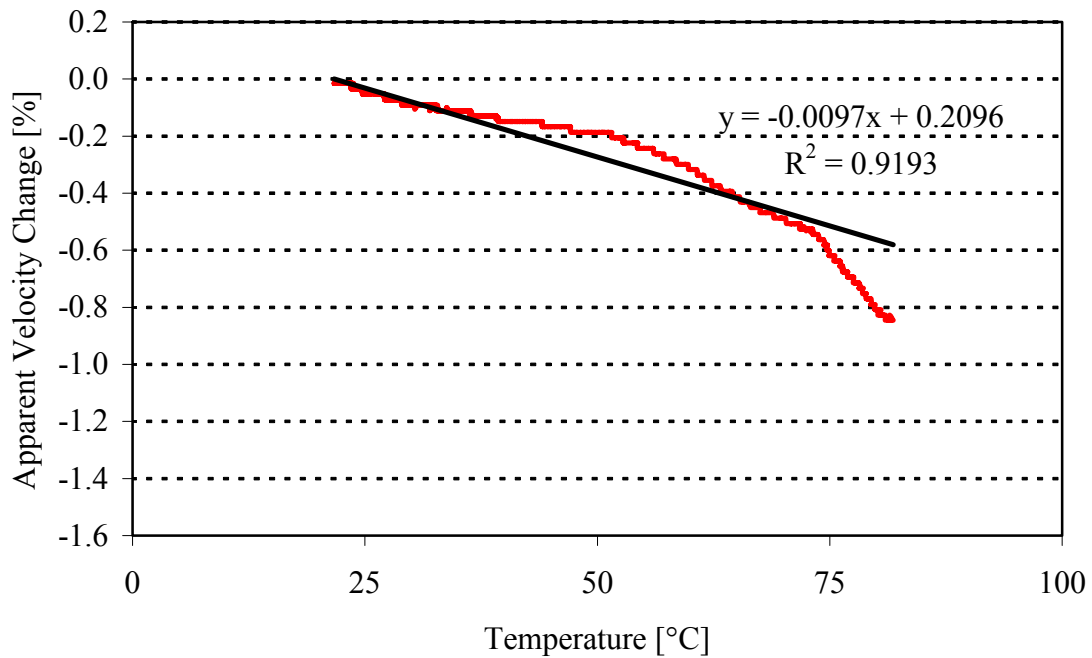


Figure 23 Apparent velocity change versus temperature in titanium with 3.1% N using a longitudinal transducer (unacceptable data).

Even without positively identifying the underlying physical mechanism or mechanisms responsible for the observed variation in the acousto-thermal coefficient, we could increase the reliability and accuracy of our results by eliminating the obvious artifacts of excessively low coefficient of determination ($R^2 < 0.95$). Figure 24 shows the distribution of the coefficient of determination versus the longitudinal acousto-thermal coefficient (β) after filtering. Even the filtered data exhibits an obvious trend of decreasing coefficient of determination, i.e., lower level of confidence in the accuracy and reliability of the data, with decreasing magnitude of the acousto-thermal coefficient. Unfortunately, increasing the threshold R^2 value used for filtering would eliminate most of the data on the difficult-to-measure Ti-N specimens of high nitrogen content, therefore further experiments are needed to increase the accuracy of these results.

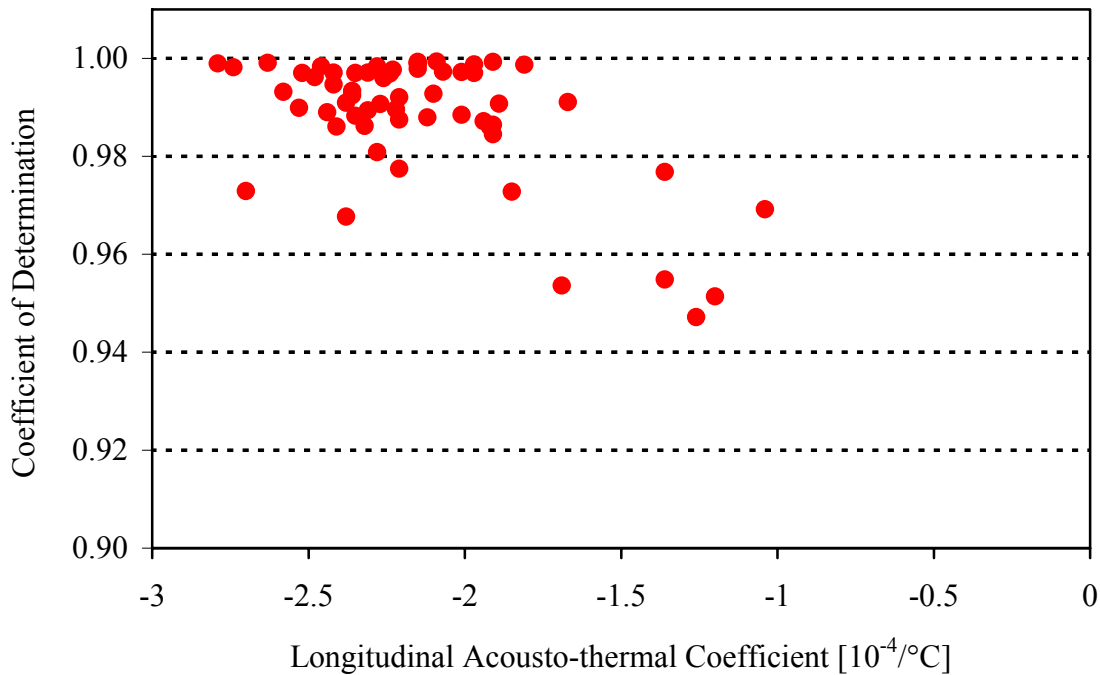


Figure 24 Distribution of the coefficient of determination (R^2) versus the longitudinal acousto-thermal coefficient (β) after eliminating the few obvious artifacts of $R^2 < 0.95$.

Figure 25 shows a graphical representation of the crucial data listed earlier in Table 5. The error bars indicate the full range of the measured values. It should be mentioned that the apparent decrease in variation shown for the 3.8% Ti-N specimen is due to the small number of successful runs (only 3) rather than to good reproducibility. Actually, the fairly strong implicit correlation illustrated in Figure 24 between increasing nitrogen content and decreasing measurement repeatability suggests that the dominating uncertainty is somehow related to the reduced consistency (micro-porosity, micro-cracks, inhomogeneous grain structure, etc.) of the Ti-N specimens. Therefore, additional measurements should be conducted on the Ti-N specimens to further investigate the possibility of increasing the measurement accuracy on these specimens by better control of the transducer and couplant parameters and by improved data acquisition.

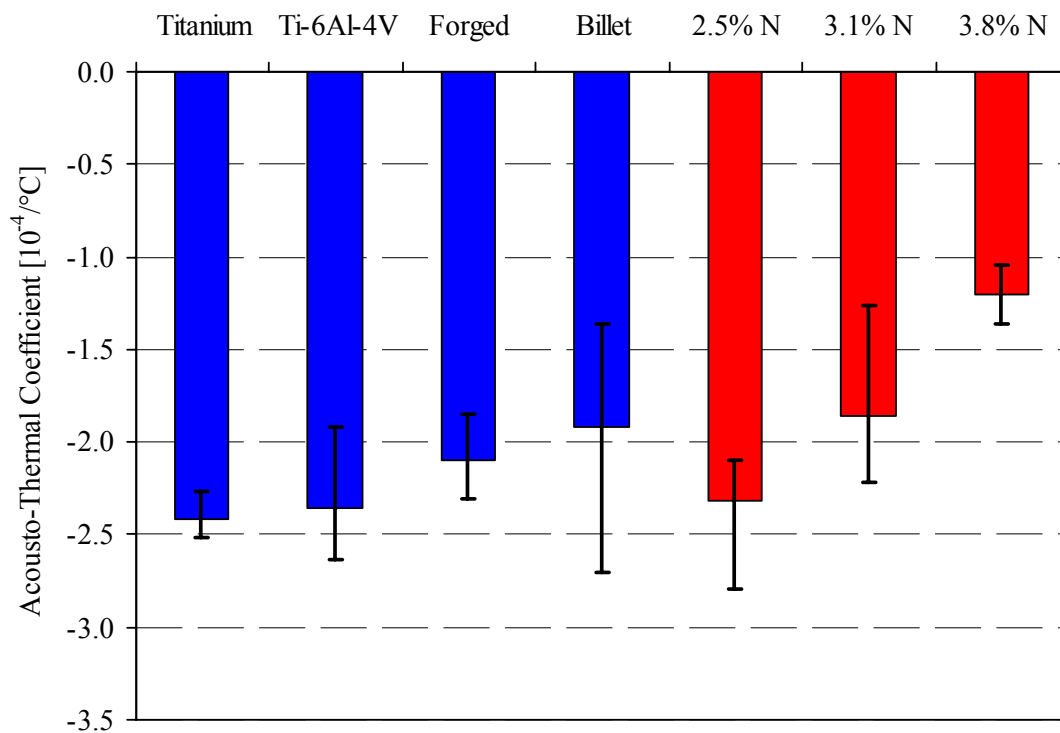


Figure 25 A graphical representation of the longitudinal acousto-thermal coefficient data listed in Table 5 (the error bars indicate the full range of the measured values).

3.4 Velocity Measurements

The longitudinal and shear velocities were measured in the titanium grade 2, Ti-6Al-4V rolled, forged and canted specimens, the titanium billet, as well as the 2.5% N, 3.1% N, and 3.8% N titanium specimens. The same setup as described previously was used because it accurately measures the absolute propagation time delay in the specimen. From this, the unperturbed velocity c_0 is easily calculated by

$$c_0 = \frac{2d_0}{t_0}, \quad (8)$$

where d_0 is the unperturbed thickness of the specimen measured by calipers and t_0 is the unperturbed two-way propagation delay measured by the Time Interval Counter. Figures 26 and 27 show that, as expected, the sound velocity in Ti-N increases by roughly 3% with each weight percent of nitrogen, which is in good agreement with the findings of previous studies [22].

The specimens with 4.8% N and 5.9% N were not measured since a usable signal could not be obtained. Even at very high gain, only the first back wall echo was clearly visible, and therefore, the method described above of obtaining the velocity could not be used. In an attempt to gather some data, two 2.25 MHz, 0.25" diameter longitudinal transducers were used in pitch-catch mode on the 5.9% N specimen. In pitch-catch mode, a transducer is placed on either side of the specimen, so that one transducer produces the pulse and the other "catches" the signal on the opposite side of the specimen. The advantage of pitch-catch mode is that the signal only travels through one thickness to the other transducer rather than bouncing from the back wall and returning to the transducer. This effectively lowers the attenuation and hopefully produces a stronger signal. A signal was established and the time delay to the first back wall echo was recorded. Next, the two transducer faces were placed against each other and the time delay was once again recorded. The difference between the time delay recorded when the specimen was in

between the transducers and when it was removed could give a rough estimate of the velocity in the Ti-5.9% N specimen from the relation

$$c_0 = \frac{d_0}{t_2 - t_1}, \quad (9)$$

where d_0 is the unperturbed thickness of the specimen measured by calipers, t_2 is the propagation delay with the 5.9% N specimen in place, and t_1 is the propagation delay with the specimen removed and the transducer faces pressed against each other, both measured by the Time Interval Counter. This estimate of the velocity in the 5.9% N specimen yielded approximately 4.2 mm/ μ s, which is considerably less than the velocity in the Ti-N specimens in Figure 26. The significantly lower velocity can only be attributed to increased porosity in the specimens. Increased porosity decreases the stiffness in a material and in turn, decreases the measured velocity. Figure 28 shows the effect of nitrogen content on the velocity in our Ti-N specimens.

Furthermore, to characterize what is meant by a weak signal, the peak-to-peak amplitude of the first back wall echo was measured in all of the titanium specimens and is shown in Figure 29. A dramatic drop in amplitude is seen in the 4.8% N and 5.9% N specimens. Again, the only reason why the amplitude in the 3.1% N specimen, for example, would be comparable to the titanium billet specimen, but the peak-to-peak amplitude in the 4.8% N specimen would be so much lower is due to the increased porosity. This complication is why these two specimens could not be used in the acousto-thermal measurements.

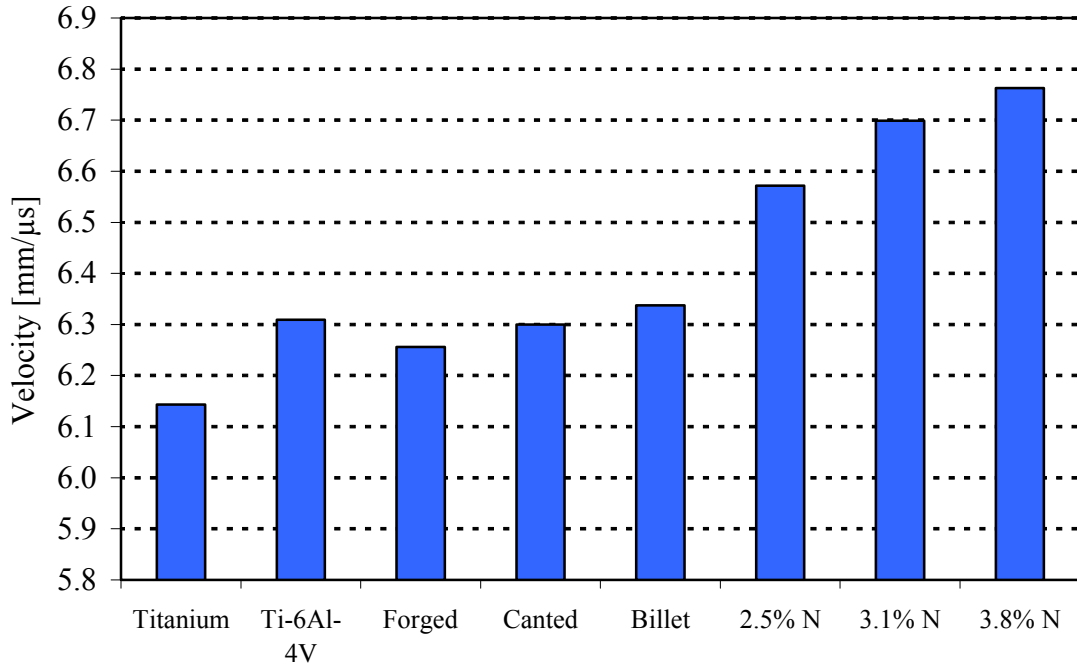


Figure 26 Longitudinal velocity in titanium with varying levels of nitrogen content.

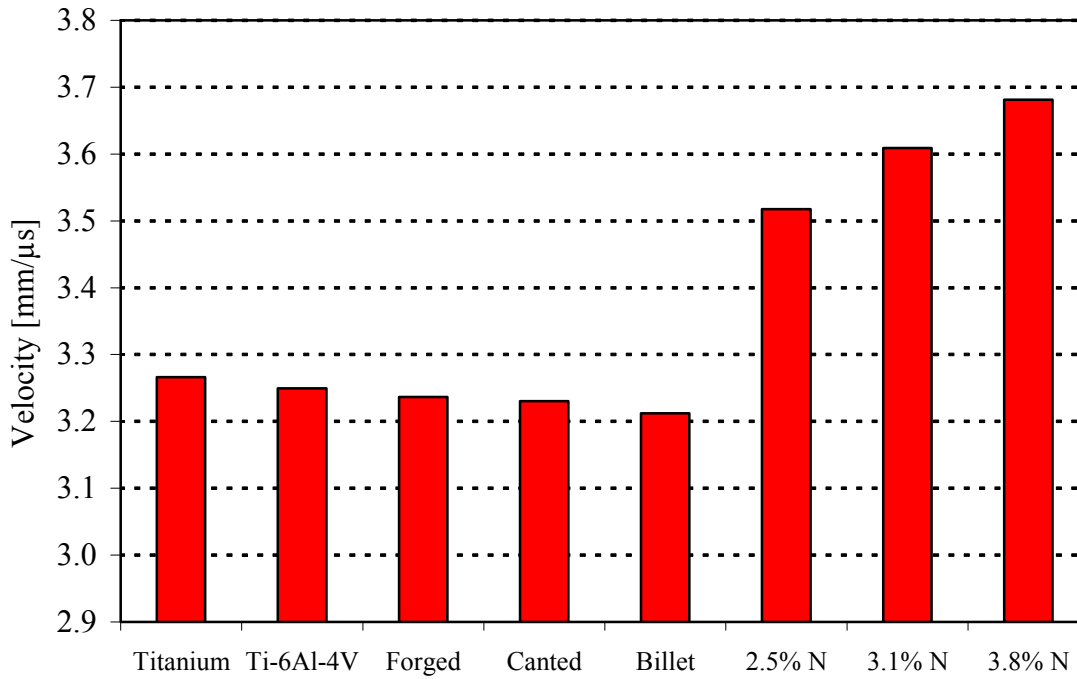


Figure 27 Shear velocity in titanium with varying levels of nitrogen content.

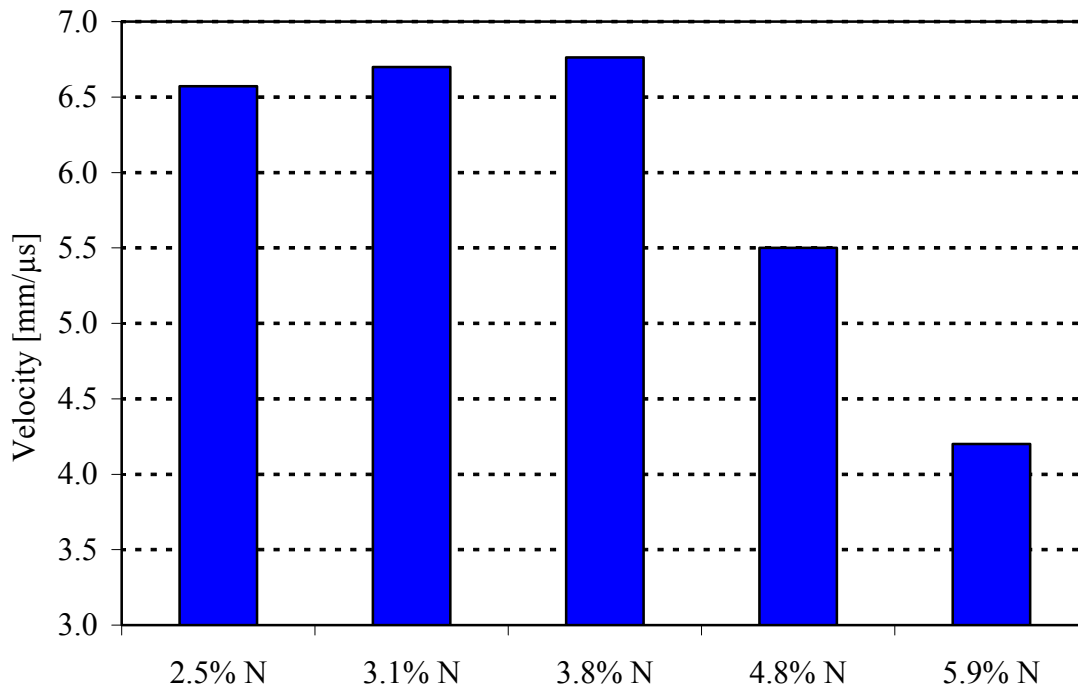


Figure 28 Longitudinal velocity versus increasing nitrogen content.

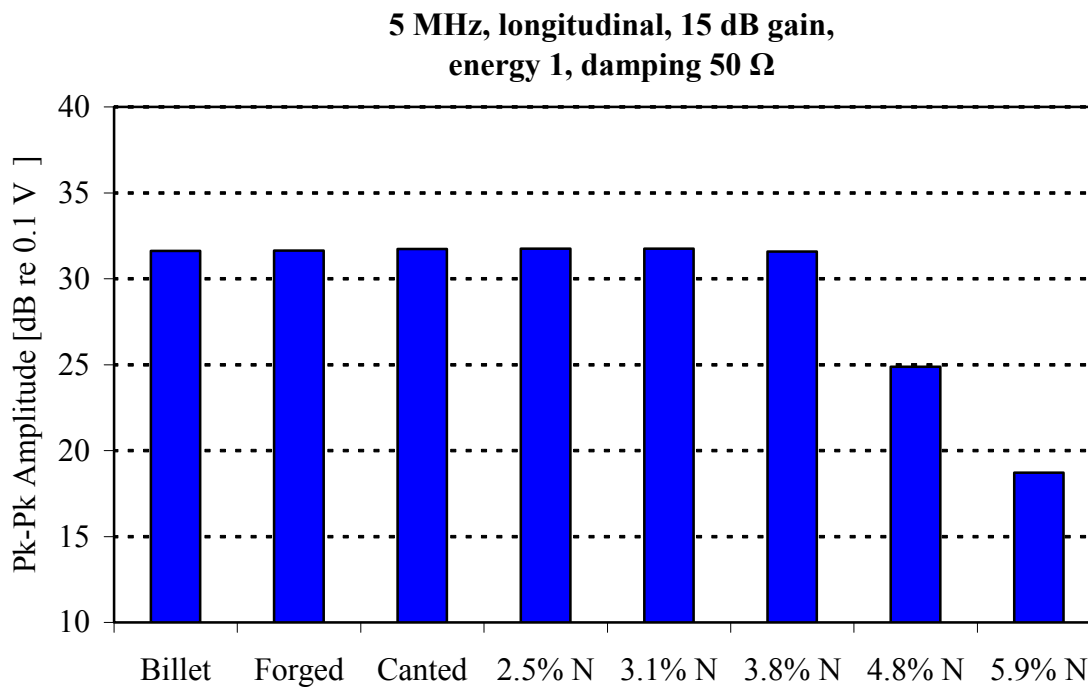


Figure 29 Peak-to-peak amplitude of the 1" titanium specimens.

4. Relative Contributions to the Overall Thermal Effect

Three factors contribute to the changing propagation time when a specimen is heated, namely the geometrical change due to thermal expansion (α), the acousto-elastic contribution (K), and the acousto-thermal contribution (β). The relative velocity change caused by each contribution can be expressed by the following formula

$$\frac{\Delta c}{c_0} = \frac{\Delta d}{d_0} - \frac{\Delta t}{t_0}, \quad (10)$$

where t is the time of arrival of the sound wave, d is the distance which the wave travels, and c is the speed of the sound. By means of a simple example, it can be determined which mechanism produces the dominating effect that should be examined further. A Ti-N specimen of 4-6% nitrogen content and a temperature change of $\Delta T = 50^\circ\text{C}$ is assumed in the following example.

The dimensional change due to unrestrained thermal expansion can be expressed as

$$\left. \frac{\Delta d}{d_0} \right|_{\text{TE}} = \alpha \Delta T, \quad (11)$$

where the thermal expansion coefficients of Ti-6Al-4V and Ti-3.8%N are known from the experiments done previously, $\alpha_{\text{Ti-6Al-4V}} \approx 10 \times 10^{-6}/^\circ\text{C}$ and $\alpha_{\text{Ti-N}} \approx 7 \times 10^{-6}/^\circ\text{C}$ (with slight overestimation of the difference to be conservative). Therefore, the expected maximum differential strain due to thermal expansion can be calculated as follows

$$\varepsilon_{\max} = \frac{\Delta d_{\text{Ti-6Al-4V}} - \Delta d_{\text{TiN}}}{d_0} \approx (\alpha_{\text{Ti-6Al-4V}} - \alpha_{\text{TiN}}) \Delta T = 1.5 \times 10^{-4}. \quad (12)$$

The corresponding maximum thermal stress can be expressed as

$$\sigma_{\max} = E \varepsilon_{\max} \approx 2.5 \text{ ksi}, \quad (13)$$

where $E = 1.65 \times 10^4$ ksi is the known modulus of elasticity in Ti-6Al-4V [18]. The acousto-elastic contribution can be expressed as follows

$$\left. \frac{\Delta c}{c_0} \right|_{AE} = K \sigma, \quad (14)$$

where $K \approx 6 \times 10^{-5}$ ksi⁻¹ denotes the magnitude of the average expected acousto-elastic coefficient of Ti-6Al-4V so that the estimated upper limit for the resulting velocity change is

$$\left. \frac{\Delta c}{c_0} \right|_{AE} \approx K \sigma_{\max} = 1.5 \times 10^{-4}, \quad (15)$$

which is the same as the value of the maximum differential thermal strain from Eq. (12).

The acousto-thermal contribution can be expressed as follows

$$\left. \frac{\Delta c}{c_0} \right|_{AT} = \beta \Delta T. \quad (16)$$

Because of the relatively low level of thermal expansion, Eq. (16) can be approximated by

$$\left. \frac{\Delta c}{c_0} \right|_{AT} \approx - \left. \frac{\Delta t}{t_0} \right|_{AT} = \beta_a \Delta T, \quad (17)$$

where β_a is the measured apparent acousto-thermal coefficient without correction for thermal expansion which is a much weaker effect (for Ti-6Al-4V $\beta_a \approx -2.3 \times 10^{-4}/^\circ\text{C}$ and $-8.9 \times 10^{-4}/^\circ\text{C}$ for longitudinal and shear waves, respectively, versus $\alpha \approx 1 \times 10^{-5}/^\circ\text{C}$).

Since the thermally induced acousto-elastic effect was found to cause only a minor relative velocity change of $\approx 3 \times 10^{-6}$ for 1°C change in temperature (see Eq. 15 for 50°C), we can conclude that the dominating effect is that of the thermal modulation of sound velocity, i.e., the acousto-thermal coefficient, and that the other contributions, namely the thermal expansion and

the acousto-elastic effects are essentially negligible. This is the reason why the acousto-thermal coefficient is emphasized in this thesis more than the other two contributions.

5. Conclusions

We have conducted thermal expansion, acousto-elastic, and acousto-thermal tests in order to assess the feasibility of thermal-elastographic detection of non-voided hard-alpha inclusions in titanium alloys. Based on our measurements, the direct thermal expansion effect and the thermally induced acousto-elastic effect are all but negligible relative to the acousto-thermal velocity change. The acousto-thermal coefficients were found to be rather sensitive to changes in nitrogen content (for simplicity, these coefficients were not corrected for thermal expansion which represents a smaller effect than the other experimental uncertainties in the measurements). Both the longitudinal and shear acousto-thermal coefficients are negative, i.e., the velocities decrease at increasing temperatures. According to our results, the longitudinal coefficient decreases while the shear coefficient increases with increasing nitrogen content. The behavior of the shear coefficient is rather surprising in light of the fact that brittle materials usually exhibit reduced elastic nonlinearity, which should decrease the temperature dependence of the shear velocity too. One possible explanation is that shear wave propagation is more affected by the presence of micro-porosity and other microstructural imperfections, which accompany the increase in nitrogen content. This porosity is also believed to be responsible for the dramatically reduced mechanical strength of the nitrogen-enriched specimens and for the fact that specimens of the highest nitrogen content could not be tested by ultrasonic means at all. It is likely that this porosity has also adversely influenced the longitudinal acousto-thermal measurements in specimens of higher than 3% nitrogen content, therefore we will have to make additional efforts to increase the accuracy and reliability of our experiments. Moreover, additional efforts will be needed to pinpoint the effect of variables, such as amount of couplant, water bath levels, thermally aging transducers, etc., on the acousto-thermal measurements.

6. Future Work

To date, all three types of nondestructive test have been verified on titanium. The acousto-elastic measurements were not performed on the embrittled Ti-N specimens because they were too small for the MTS and their mechanical strength was highly questionable. The 1"-long specimens could most likely be tested in compression and it would require an extensive setup preparation. Since it was shown earlier that the relative contributions of the thermal expansion and acousto-elastic coefficients were small compared to the acousto-thermal coefficient, it was not considered a serious limitation that the Ti-N specimens could not be tested in the MTS.

In light of our previous findings, all the focus now has been placed on the further improvement of the acousto-thermal measurements that were found to be crucial for the feasibility of thermal-elastographic detection of non-voided hard-alpha inclusions in titanium alloys. As mentioned before, these tests are tedious and complicated, which can often lead to spurious artifacts and, ultimately, incorrect results. Many precautions have been taken to ensure that the tests are repeated in a similar manner. Intrinsic measurement uncertainties include electrical noise, mechanical vibrations, thermal instability, long-term drift, etc. Possibly, the lack of sufficient reproducibility is caused by aging of the ultrasonic transducers and imperfect coupling to the specimens, while instrument anomalies and imperfections appear to be under control. Many tests have been discarded because of spurious spikes in the data, noise from the MTS when in use by another student, or a nonlinear velocity versus temperature curve. Explaining why a particular test went wrong is nearly impossible, but knowing that it did go wrong is easy. However, suggested for future work is a study to understand the effect of

different amounts of couplant, different water levels, and different transducers that may have lost stability and sensitivity after being heated several times.

The longitudinal measurements seem to be easier than the shear measurements. The water is allowed to air-cool from 80°C to room temperature whereas the water is cooled by the chiller to 5°C in the shear measurements. This factor seems to produce a noticeable curve in most of the shear plots at the same point in the temperature range. This is believed to be a serious limitation for the shear measurements. More focus was directed toward the longitudinal results because the acousto-thermal coefficient was determined in what was deemed to be a more accurate way. However, this method for the shear measurements must be used because of the viscosity loss of shear couplants that were discussed previously. It would be beneficial to investigate another method to perform the shear acousto-thermal measurements so as to verify our findings of an increasing acousto-thermal coefficient with increasing nitrogen. Additional results on the loss of coupling in shear measurements are presented in Appendix 2.

Bibliography

- [1] Brasche, L.J.H., and Buck, O., “Nondestructive Methods for Determination of Mechanical Properties of Aluminum and Titanium Alloys,” *Review of Progress in Quantitative Nondestructive Evaluation*, Vol. 10B, 1991, pp. 1701-1706.
- [2] Chan, K.S., Perocchi, L., and Leverant, G.R., “Constitutive Properties of Hard-Alpha Titanium,” *Metallurgical and Materials Transactions*, Vol. 31A, 2000, pp. 3029-3040.
- [3] Schafrik, R., and Sprague, R., “Saga of Gas Turbine Materials, Part I,” *Advanced Materials and Processes*, Vol.162, No.3, 2004, pp. 33-36.
- [4] Haynes, A., “The Crash of United Flight 232,” NASA Ames Research Center Dryden Flight Research Facility, California, May 1991.
[<http://www.panix.com/~jac/aviation/haynes.html>. Accessed 10/18/04.]
- [5] “National Transportation Safety Board Aircraft Accident Report AAR-90/06,” November 1990. [<http://amelia.db.erau.edu/reports/ntsb/aar/AAR90-06.pdf>. Accessed 10/18/04.]
- [6] “Human Factors in Aviation Maintenance and Inspection,”
[<http://hfskyway.faa.gov/document.htm>. Accessed 10/18/04.]
- [7] “Engine Titanium Consortium,”
[<http://aar400.tc.faa.gov.aar4304/430Programs/AgingAircraft/AircraftEngines/aircraftengines>. Accessed 10/18/04.]
- [8] Bartos, J.L., Copley, D.C., Gilmore, R.S., and Howard, P.J., “Advanced Ultrasonic Inspection Techniques for Titanium Billet Materials,” *Titanium '95: Science and Technology*, Vol. 2, 1996, pp. 1513-1520.
- [9] “Hard Alpha Inclusion Detection,” NDT Update, Vol. 13, No. 12, 2004.
- [10] “Feasibility Study of Thermal-Elastographic Detection of Non Voided Hard Alpha Inclusions in Titanium Alloys,” proposal submitted by Honeywell Engines, Systems, and Services/University of Cincinnati.
- [11] Gigliotti, M.F.X., Gilmore, R.S., and Perocchi, L.C., “Microstructure and Sound Velocity of Ti-N-O Synthetic Inclusions in Ti-6Al-4V,” *Metallurgical and Material Transactions*, Vol. 25A, 1994, pp. 2321-2329.
- [12] Ponnekanti, H., Ophir, J., Huang, Y., and Cespedes, I., “Fundamental Mechanical Limitations on the Visualization of Elasticity Contrast in Elastography,” *Ultrasound in Med. & Biol.*, Vol. 21, No. 4, 1995, pp. 533-543.

- [13] Ophir, J., Cespedes, I, Ponnekanti, H., Yazdi, Y., and Li, X., "Elastography: A Quantitative method for Imaging the Elasticity of Biological Tissues," *Ultrasonic Imaging*, Vol. 13, 1991, pp.111-134.
- [14] Barron, T.H.K., "Generalized Theory of Thermal Expansion of Solids," *Thermal Expansion of Solids*, edited by C.Y. Ho, Vol. I-4, CINDAS Data Series on Material Properties, ASM International, Materials Park, 1998, pp. 1-105.
- [15] Ruffino, G., "Historical Perspective," *Thermal Expansion of Solids*, edited by C.Y. Ho, Vol. I-4, CINDAS Data Series on Material Properties, ASM International, Materials Park, 1998, pp. 135-153.
- [16] Gaal, P.S., "Pushrod Dilatometers," *Thermal Expansion of Solids*, edited by C.Y. Ho, Vol. I-4, CINDAS Data Series on Material Properties, ASM International, Materials Park, 1998, pp. 165-179.
- [17] White, G.K., "Thermal Expansion of Reference Materials," *Thermal Expansion of Solids*, edited by C.Y. Ho, Vol. I-4, CINDAS Data Series on Material Properties, ASM International, Materials Park, 1998, pp. 269-284.
- [18] See, e.g., www.matweb.com.
- [19] Nagy, P.B., "Nonlinearity," *Ultrasonic Nondestructive Evaluation*, University of Cincinnati, 2003, pp. 1-21.
- [20] Kobori, O., and Iwashimizu, Y., "Effects of Stress and Temperature on Ultrasonic Velocity," *Elastic Waves and Ultrasonic Nondestructive Evaluation*, edited by Datta, S.K., Achenbach, J.D., and Rajapakse, Y.S., North Holland, 1990, pp. 339-343.
- [21] Ruiz, A., and Nagy, P.B., "SAW Dispersion Measurements for Ultrasonic Characterization of Surface-Treated Metals," *Instrumentation, Measurement and Metrology*, Vol. 3, 2003, pp. 59-85.
- [22] Margetan, F.J., Gigliotti, M., Brashe, L., and Leach, W., "Fundamental Studies: Inspection Properties for Engine Titanium Alloys," FAA final report DOT/FAA/AR-02/114, 2002.

8. Appendix

8.1 Appendix 1

Detailed Setup for Time Delay Measurements

Pulser/Receiver:

Model: pulse/echo

LPF: 10 MHz

HPF: 1 MHz

These settings can vary; a combination was chosen that produces a fairly large signal.

Gain [dB]: whatever needed to obtain a decent signal

Damping: 3 (50 Ω)

Energy: 1

PRF: 1 kHz (acousto-elastic measurements), 2 kHz (acousto-thermal measurements)

Digital Delay/Pulse Generator:

Use only the "Delay" button to set the arm.

A is the time needed to set the arm just before the positive zero crossing of the front wall echo.

B is the time needed to set the arm just before the positive zero crossing of the back wall echo.

Universal Time Interval Counter:

Mode: Time

Source (Start): A

Gate/Arm: +Time, Ext, Comp/Hldf

Sample Size: 1000 (acousto-elastic measurements), 500 (acousto-thermal measurements), Auto

Display: Mean

Scale: This factor is changed according to how much the time delay changes with temperature for each specimen. A bigger scaling factor means less change in the voltage signal read by the computer. The signal can only be 0-8 V, so the scaling factor needs to be changed accordingly such that the signal does not saturate.

Gate: Pos, Arm

Start: +, DC

Stop: +, DC

8.2 Appendix 2

Acousto-Thermal Shear Wave Couplant Study

As mentioned before, two types of shear couplant were used in the acousto-thermal measurements, namely honey and a high-viscosity Panametrics shear wave couplant. It was found that both lose viscosity at high temperatures. However, honey also dissolves in water in addition to losing viscosity with increased temperature. This means that around 55-60°C the signal on the oscilloscope disappears and will not come back because the honey is dissolved. The advantage to using the Panametrics shear wave couplant is that it does not dissolve in water. The signal disappears just like in the case of honey at a similar temperature, but if the water is cooled back down below 55-60°C, the signal reappears. However, removing the couplant from the transducer requires an unpleasant solvent like acetone.

A couplant study was done with the same Pyrex dish as described in the acousto-thermal setup. First, the peak-to-peak amplitude of a signal was recorded via a Labview program on a specimen for twenty minutes. Honey was used as the shear wave couplant. The peak-to-peak amplitude can be displayed on the oscilloscope and sent to a Labview program via an RS-232 interface. In order to illustrate how fast the thin honey layer between the transducer and the specimen is dissolved by water even at relatively low temperatures, the specimen was placed in room-temperature water while still recording the amplitude. The amplitude starts to decrease within ≈ 50 minutes of placing the specimen in the water and eventually disappears after approximately three hours. Figure A2.1 shows the peak-to-peak amplitude as a function of time.

The important part of the graph is the shape of the decreasing amplitude. It very well could take a shorter or longer time for the honey layer to dissolve in water based on how long the transducer was clamped on the specimen before being placed in water. The Panametrics shear

wave couplant was also tested in the same manner as the honey, but did not lose amplitude when placed in room-temperature water, although the specimen was left in the water over the period of three days.

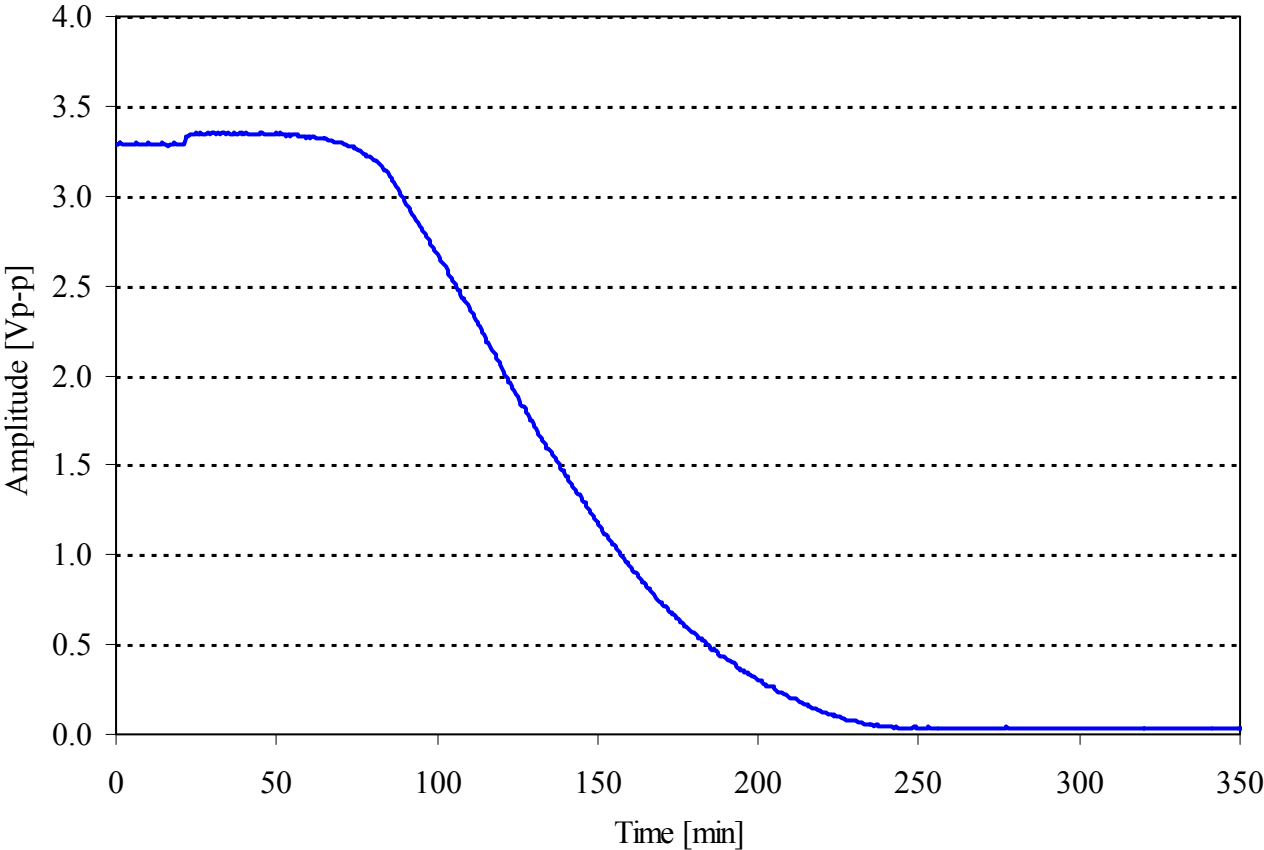


Figure A2.1 Peak-to-peak amplitude versus time of a specimen placed in a room-temperature water bath using honey as the shear wave couplant.